Discovery at the Interface of Science and Engineering:

Science Matters!

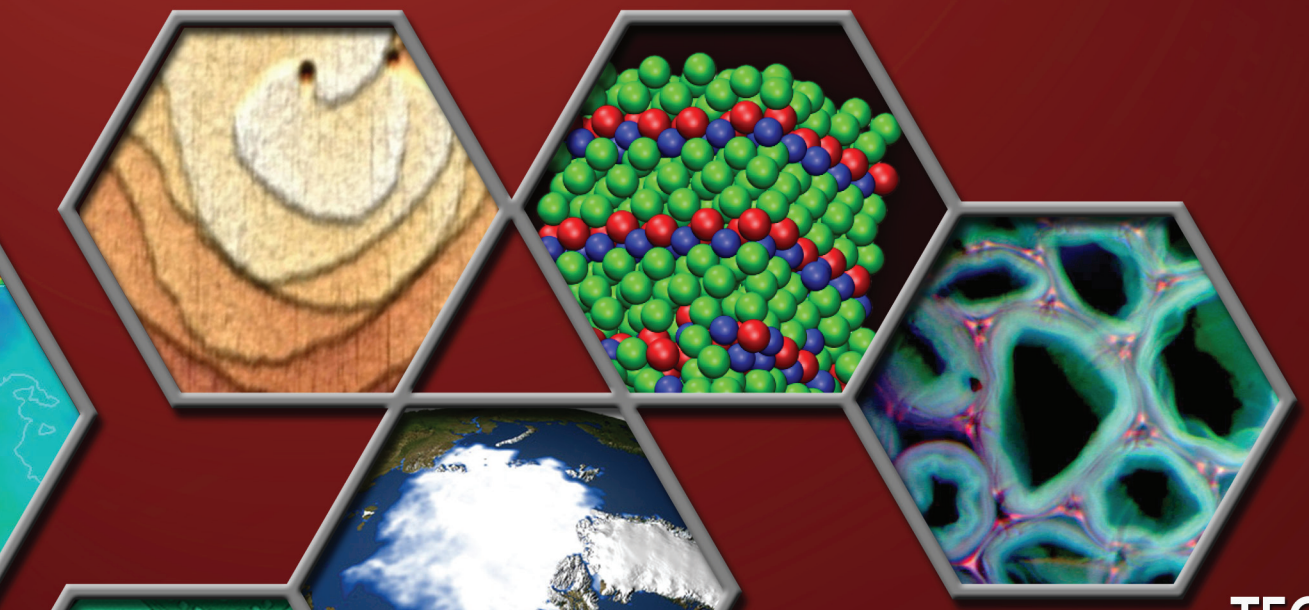

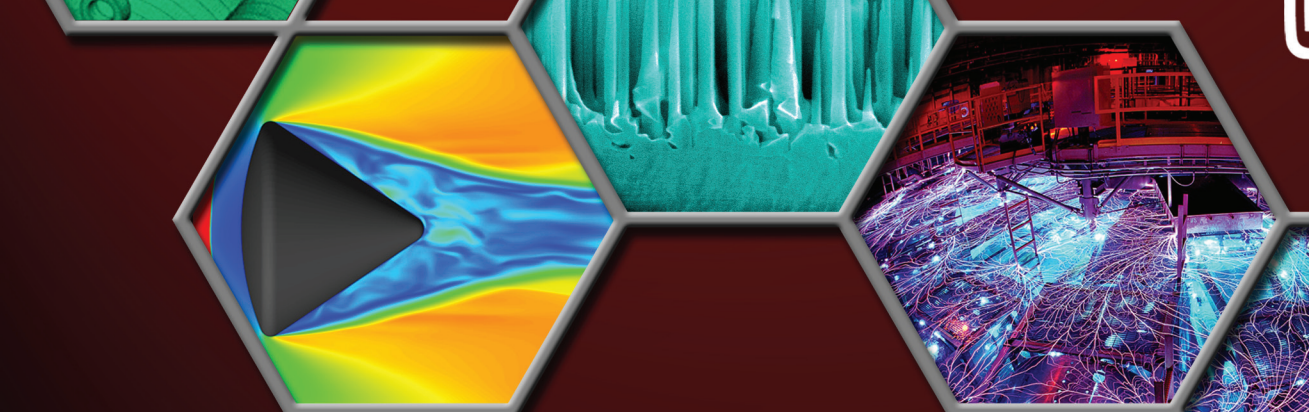

SCIENCE, TECHNOLOGY & ENGINEERING

MARCH, 2010

Sandia National Laboratories

NOTICE: This report was prepared as an account of work sponsored by an agency of the United States Government. Neither the United States Government, nor any agency thereof, nor any of their employees, nor any of their contractors, subcontractors, or their employees, make any warranty, express or implied, or assume any legal liability or responsibility for the accuracy, completeness, or usefulness of any information, apparatus, product, or process disclosed, or represent that its use would not infringe privately owned rights. Reference herein to any specific commercial product, process, or service by trade name, trademark, manufacturer, or otherwise, does not necessarily constitute or imply its endorsement, recommendation, or favoring by the United States Government, any agency thereof, or any of their contractors or subcontractors. The views and opinions expressed herein do not necessarily state or reflect those of the United States Government, any agency thereof, or any of their contractors.

Printed in the United States of America. This report has been reproduced directly from the best available copy.

SAND2010-0879P 03/2010
Issued by Sandia National Laboratories, Albuquerque, New Mexico, USA for the US National Nuclear Security Administration (NNSA) Office of Research & Development for National Security Science & Technology, NA-121.

Sandia is a multiprogram laboratory operated by Sandia Corporation, a Lockheed Martin Company, for the United States Department of Energy's National Nuclear Security Administration under contract DE-AC04-94AL85000.

Discovery at the Interface of Science and Engineering: **Science Matters!**

SANDIA NATIONAL LABORATORIES

Science, Technology and Engineering

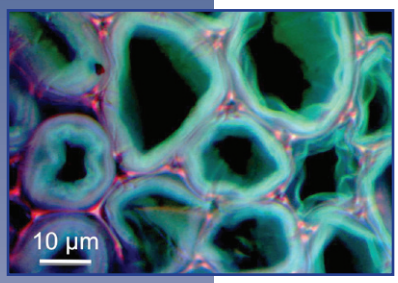

Bioscience

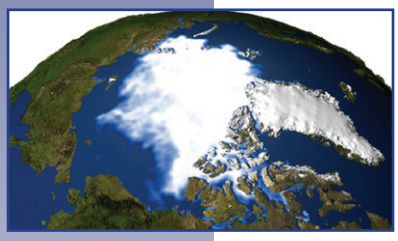
Computers and Information Sciences

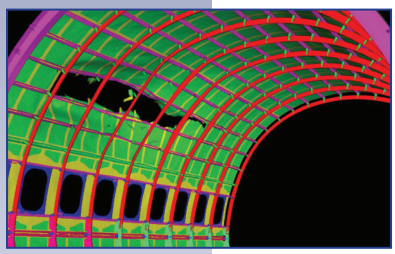
Engineering Sciences

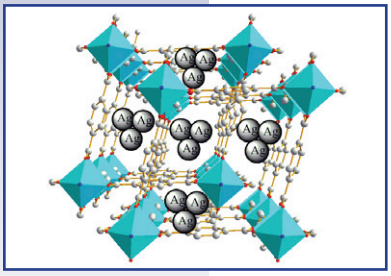
Materials Science and Technology

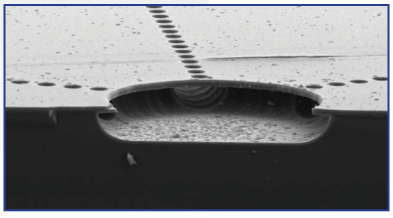
Microelectronics and Microsystems


Pulsed Power

Vision

Sandia National Laboratories is the provider of innovative, science-based, systems-engineering solutions to our Nation's most challenging national security problems.

Mission

Committed to "science with the mission in mind," Sandia creates innovative, science-based, systems-engineering solutions that

- sustain, modernize, and protect our nuclear arsenal,
- prevent the spread of weapons of mass destruction,
- provide new capabilities for national defense,
- defend against terrorism,
- protect our national infrastructures, and
- ensure stable sources of energy and other critical resources.

Guiding principles for ST&E

- Ensure that the fundamental science and engineering core is vibrant and pushing the forefront of knowledge
- Enable the programs by effective application of that science base
  - responding to current needs
  - anticipating the future

About *Science Matters!*

The purpose of ***Science Matters!*** is to publicize and celebrate recent Sandia accomplishments in science, technology, and engineering. We feature the science that underpins and enables technology for Sandia's missions. We nurture expertise, facilities and equipment to create world-class science that pushes the frontiers of knowledge and anticipates future mission needs. New ***Science Matters!*** are being issued semiannually.

Vice President & Chief Technology Officer
J. Stephen Rottler, Ph.D.
505-844-3882
jsrottl@sandia.gov

Deputy, Science & Technology
James Woodard, Ph.D.
505-845-9520
jwoodar@sandia.gov

***Science Matters!* Point of Contact**
Alan Burns, Ph.D.
505-844-9642
aburns@sandia.gov

Sandia National Laboratories

National Nuclear Security Administration

FIGURE CAPTIONS

(Preceding page, from top to bottom)

Confocal fluorescence microscope image of switchgrass cell wall

Composite image of sea ice in the Arctic region acquired in 2003 by the Defense Meteorological Satellite Program Special Sensor Microwave Imager. Source: earthobservatory.nasa.gov

Simulation results showing tearing in an aircraft fuselage subjected to blast loading. Failure is represented using the "element death" technique.

Silver nanoparticles created in a metal organic framework (MOF).

Wet hydrogen fluoride etched buried guidance cues for neural networks on silicon chip. Scale bar = 10 µm.

Lightening caused the 2006 Sago mine disaster in West Virginia.

Contents

Bioscience
Biofuels

Unlocking the Keys to Next-Generation Biofuels: Advanced Pretreatment Technology

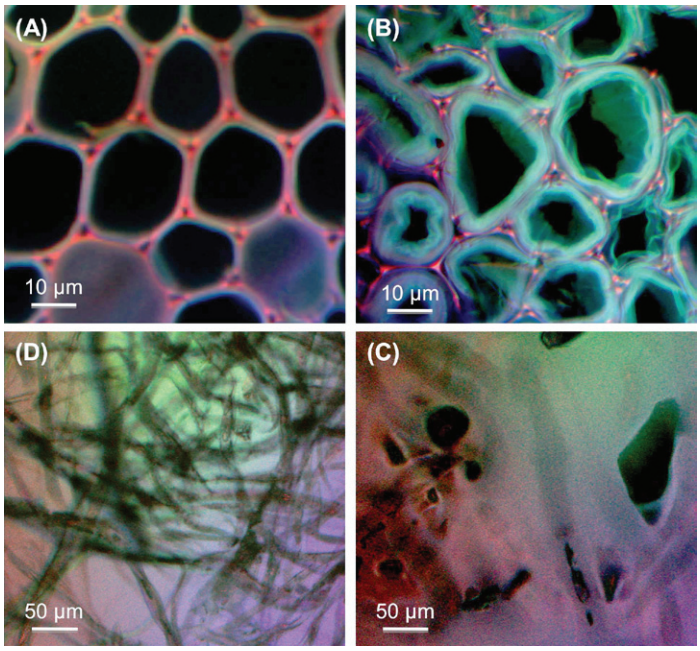

Figure 1: Confocal fluorescence images of switchgrass cell wall, (A) before pretreatment and (B) swollen cell wall after 10 min pretreatment with ethyl methyl imidazolium acetate at 1208 °C. Highly-polar ionic liquids are very effective in solvating cellulosic biomasses due to hydrogen bond formation between hydroxyl group hydrogen atoms in the cellulose and ionic liquid anions. (C): *In situ* examination three hours after pretreatment. Confocal optical slice showing cellulose regeneration after anti-solvent (water) addition into ionic liquid-solubilized switchgrass. (D): Product recovery. Regenerated non-fluorescent cellulose appears to reject lignin and appear as dark fibers in the lignin–ionic liquid fluorescent solution.

As a partner in the Joint BioEnergy Institute, Sandia is working to advance the technology of efficient biofuel production.

For more information:

Technical Contact:
Blake Simmons
925-294-2288
basimmo@sandia.gov

Science Matters Contact:
Alan Burns
505-844-9642
aburns@sandia.gov

Transportation fuels are the largest end use of energy by sector in the U.S. A full two-thirds of the world's petroleum resources are used for transportation, and 60% of that is used for ground transportation. Petroleum production is predicted by many experts to peak within ten to thirty years, after which time worldwide production will decline until resources are exhausted, resulting in dramatically higher fuel costs and potentially disastrous geopolitical conflicts for resources. What's more, each gallon of gasoline and diesel produces an astonishing twenty pounds of CO_2 (resulting in an average of seven tons per vehicle per year); thus the millions of vehicles used globally are contributing significantly to climate change.

As liquid fuels derived from solar energy and carbon stored in renewable plant biomass, biofuels are becoming increasingly important alternatives to petroleum. Recently, the Department of Energy's Office of Science established Bioenergy Research Centers to advance the development of the next generation of biofuels. One such center, the Joint BioEnergy Institute (JBEI), is a San Francisco Bay Area partnership that is led by Lawrence Berkeley National Laboratory and includes Sandia, the University of California campuses of Berkeley and Davis, the Carnegie Institution for Science, and Lawrence Livermore National Laboratory. JBEI's primary scientific mission is to focus on three key areas: feedstock (biomass) production, deconstruction of the feedstock, and fuels synthesis.

Most current pretreatments for enhancing the deconstruction of the lignocellulose component of biomass utilize acids that result in an overall loss of sugars. These acids also yield toxic by-products that inhibit the biofuel fermentation process, again resulting in an overall loss of sugars. Thus successful

commercial production of advanced biofuels will require new pretreatment approaches that enhance cellulose conversion to sugars and minimize the formation of toxic by-products, as well as new enzymes that are capable of efficiently deconstructing both the sugar and lignin components of plant cell walls. Sandia researchers in JBEI's Deconstruction Division are developing better methods to "pretreat" lignocellulose in order to enhance its deconstruction into fermentable sugars. The focus is on the use of ionic liquids, salts that are liquid rather than crystalline close to room temperature. Ionic liquid pretreatments have been proven to significantly enhance the rate of hydrolysis of cellulose, but they require large amounts of antisolvent (a solvent in which the product is insoluble) to recover the amorphous cellulose. Furthermore, a portion of the sugars may be lost to the antisolvent phase, particularly if water is used. Researchers are investigating both the effects of ionic liquids on biomass and the recovery of sugars from the ionic liquid/biomass liquor.

To generate the first published results [1], Sandia researchers used advanced imaging techniques such as confocal fluorescence microscopy to reveal how the ionic liquids interact with and disrupt the plant cell walls of switchgrass (Figure 1). From these images, it is observed that the ionic liquid completely dissolves the plant cell walls of switchgrass and generates a product that is more readily converted into sugar due to decreased lignin content and decreased cellulose crystallinity. These results pave the way for further development of the ionic liquid technology to produce a cheap, robust, and environmentally friendly route of converting biomass into biofuel.

Reference

1. Seema Singh, Blake A. Simmons, and Kenneth P. Vogel, Visualization of Biomass Solubilization and Cellulose Regeneration During Ionic Liquid Pretreatment of Switchgrass, *Biotechnology and Bioengineering*, 104 (2009) 68-75.

Computer and Information Science
Climate Change

High-Resolution Arctic Sea Ice Modeling

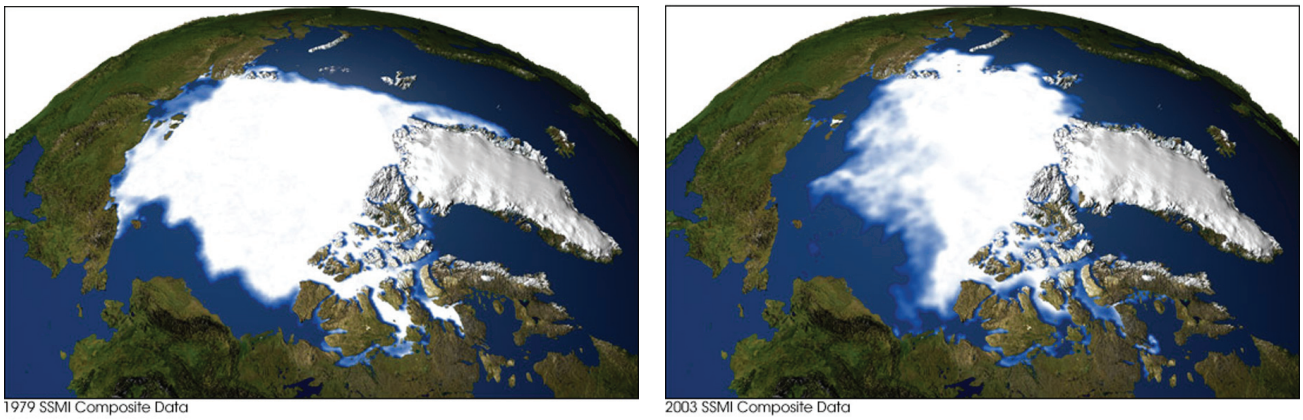

Figure 1: Composite images of sea ice in the Arctic region acquired by the Defense Meteorological Satellite Program Special Sensor Microwave Imager for 1979 (left) and 2003 (right). Source: earthobservatory.nasa.gov

Sandia is examining critical environmental parameters needed to accurately predict the behavior of sea ice due to global warming

For more information:

Technical Contacts:
Kara Peterson
505-844-9372
kjpeter@sandia.gov

Pavel Bochev
505-844-1990
pbboche@sandia.gov

Biliana Paskaleva
505-284-8783
bspaska@sandia.gov

Science Matters Contact:
Alan Burns
505-844-9642
aburns@sandia.gov

Climate change is having a disproportional impact in the Arctic due in part to complex positive feedback mechanisms involving the reflectivity and insulating properties of sea ice. As sea ice is lost, the underlying ocean is exposed to the atmosphere causing more solar radiation to be absorbed, which in turn causes further warming. The composite images of sea ice in the Arctic region shown in Figure 1 clearly demonstrate the retreat of sea ice from 1979 to 2003. Loss of sea ice facilitates recovery of previously inaccessible natural resources that may increase the possibility of international conflicts. Therefore, given the important role of sea ice in climate change and the geopolitical importance of the Arctic, high-fidelity sea ice simulations to support science-based policy making are essential.

The development and analysis of high-resolution sea ice models pose a number of serious modeling and simulation challenges. The codes used to predict the behavior of sea ice combine complex physical models for melting and growth due to radiative forcing as well as motion and deformation due to ocean current and wind forcing. The solutions can be affected by uncertainties in the forcing data, errors due to simplifications in the physical models, and errors resulting from the numerical solution methods. In conjunction with the Dept. of Energy's Office of Biological and Environmental Research Climate Research Project, Sandia researchers are addressing these sources of error by considering new physical models for the ice, developing improved numerical algorithms for their solution, and quantitatively evaluating the sensitivities of the models to input parameters.

Existing sea ice models are made up of dynamic and thermodynamic components that include a two-dimensional momentum equation for ice velocity, a constitutive model for ice internal forces, a one-dimensional heat equation for ice column temperature, and an evolution equation for ice thickness distribution. The LANL model CICE represents the state-of-the-art in sea ice modeling and has been designed to couple with the ocean and atmosphere components in the Community Climate System Model maintained by the National Center for Atmospheric Research. However, CICE has several limitations. First, the

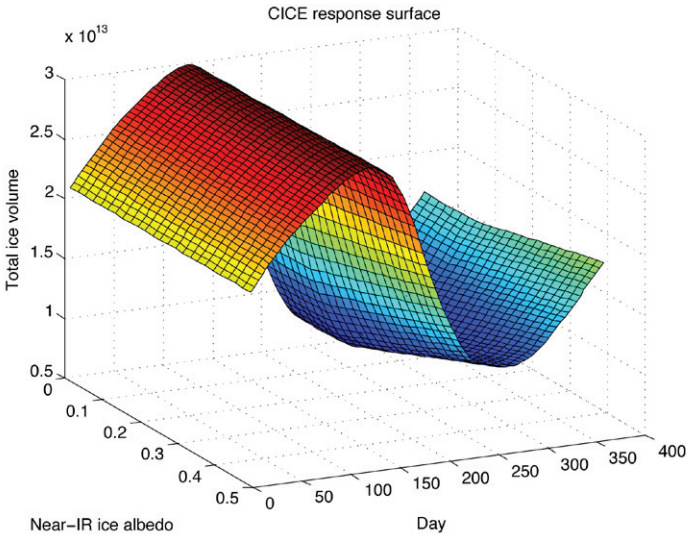

Figure 2: Single-parameter Dakota study performed with the LANL's CICE code. The response surface corresponds to the total ice volume as function of the near-IR ice albedo, and the day of the year.

constitutive model assumes that the response of ice to forcing is isotropic; this results in non-physical deformations for regions dominated by a large crack or other linear features. Second, the numerical methods used to solve the sea ice dynamics equations result in artificial diffusion and dispersion that cause smearing of the ice edge. Another approach, based on a code developed at the University of New Mexico, is designed to overcome these limitations by using an elastic-decohesive constitutive model solved with the Material-Point Method (MPM). It uses both Lagrangian particles to facilitate the discretization of the advection term in the dynamics equations and an anisotropic constitutive model that explicitly includes cracks.

Any predictive sea-ice model necessarily involves a large number of material and environmental parameters that are inherently uncertain. As a first step towards a quantitative characterization of the resulting simulation uncertainty, Sandia is evaluating the sensitivity of both the CICE and the MPM models with respect to these parameters. This allows researchers to rank the relative importance of different parameters for the propagation of uncertainties in a model and provide the means to reduce the dimension of the parameter space in an uncertainty quantification process. For this task, Arctic basin-wide simulations are being performed and the response of overall sea ice volume and area to parameters such as albedo, emissivity, and density are being evaluated. These sensitivity analyses rely on Sandia's DAKOTA (Design Analysis Kit for Optimization) sampling tools and leverage the laboratory's significant knowledge base in uncertainty quantification. A typical response surface obtained by a single-parameter DAKOTA study using the CICE model is shown in Figure 2. In this example, the surface corresponds to the total ice volume in the Arctic region plotted as function of the near-Infra-Red (IR) ice albedo, and the day of the year. The study reveals a weakly nonlinear response for albedo values between 0.0 and 0.15, followed by a transition to a linear response for values between 0.15 and 0.5. Comparison of the ice thickness plots for near IR ice albedo of 0.1 and 0.5, shown in Fig. 3, demonstrates substantial qualitative differences caused by the variation in this parameter. Similar DAKOTA studies are underway for the MPM model. Comparison of the sensitivities of the two sea ice models will help to increase confidence in their predictive capabilities and improve our understanding of the complex interactions between various parameters.

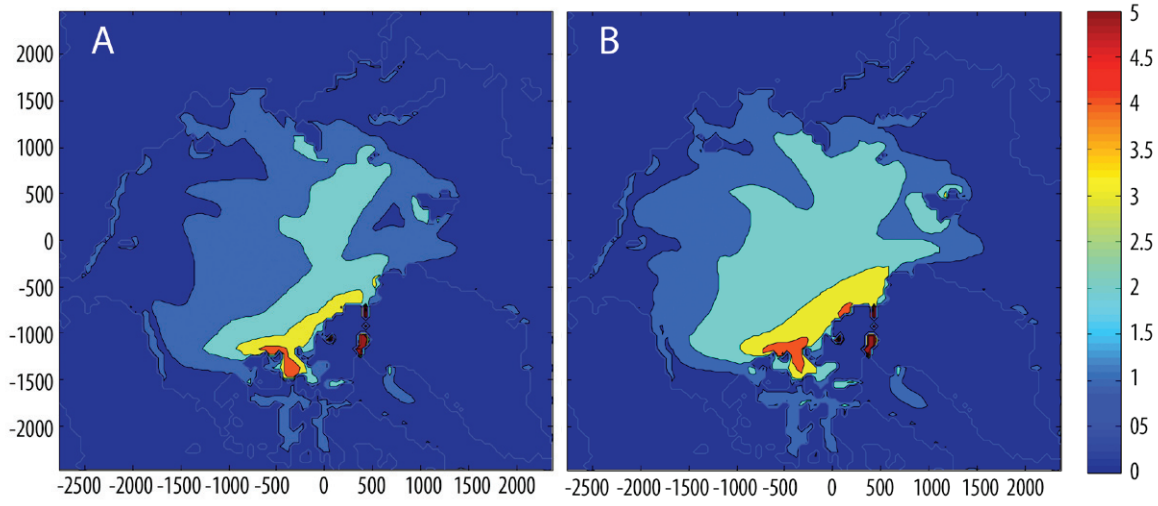

Figure 3: Dependence of sea ice thickness (meters) on near-IR ice albedo. (A) Ice thickness for high levels of near-IR absorption (near-IR ice albedo of 0.1). (B) Ice thickness for low levels of near-IR absorption (near-IR ice albedo of 0.5).

Computer and Information Sciences
Materials Simulations

Two-Temperature Model of Radiation Damage

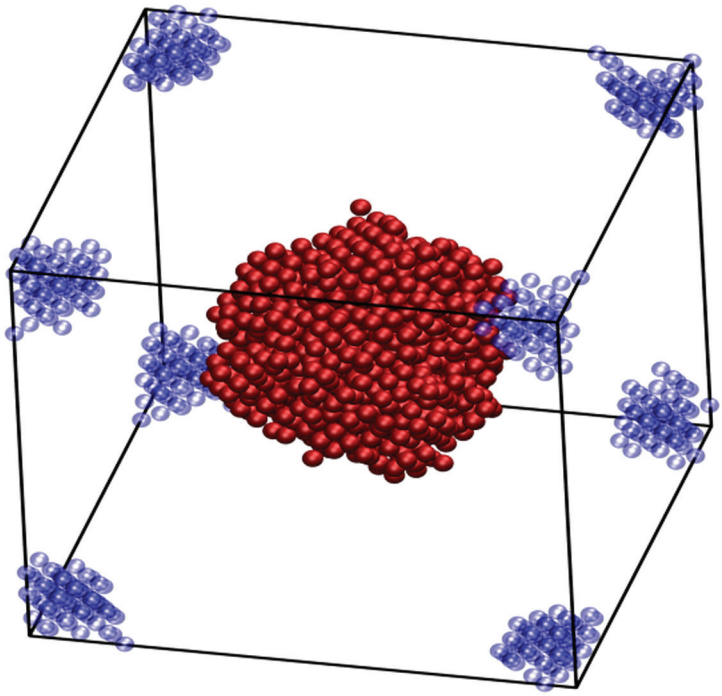

Figure 1: The initial state of the radiation-damaged system. The simulation box is the size of a 17×17×17 FCC unit cell system. The red liquid spot at the center initially consists of 1174 atoms. The 458 atoms that are tightly coupled to an infinite heat reservoir at a very low temperature are shown at the corners of the simulation cell (they form a sphere in periodic space). The 17,930 atoms that are neither defect atoms nor heat sink atoms are not shown.

Simulating radiation damage will provide more insights for the improvement of radiation-resistant circuitry

For more information:

Technical Contact:
Paul S. Crozier
505-845-9714
pscrozi@sandia.gov

Science Matters Contact:
Alan Burns
505-844-9642
aburns@sandia.gov

Electronic circuits that are resistant to low or high dose radiation damage are vital to Sandia's missions in nuclear weapons and satellites. Advances in radiation hardening technology will require better understanding of the atomistic details of radiation damage processes. Molecular simulation is a powerful tool for exploring such atomistic processes, but current methods neglect essential effects of energized electrons. These effects can be included in classical molecular dynamics (MD) simulations by coupling the atom motions to a continuum representation of the electrons through a two-temperature model (TTM) [1-3], in which the electronic subsystem is represented with the heat equation solved on a grid to mimic the thermal response of the excited carrier electrons. The two subsystems are coupled through TTM-prescribed energy exchanges. Previous work has demonstrated TTM coupling by using an inhomogeneous and finite Langevin thermostat [3].

TTMs attempt to capture the interplay between electrons and atoms in a material during thermal transients such as radiation damage by modeling the electrons and the atoms as two separate systems, with two separate temperatures that are able to exchange energy through frictional forces applied to the atoms. In collaboration with the University of Michigan (involving a DOE Computational Science Graduate Fellow), Sandia has improved the simulations by introducing an energy-conserving version of the TTM to communicate energy between the electronic and atomic subsystems. This modification allows the inhomogeneous TTM to be used for longer and larger simulations, as well as for simulations of small energy phenomena, without introducing nonphysical energy fluctuations that may affect simulation results.

Sandia National Laboratories

LDRD LABORATORY DIRECTED RESEARCH & DEVELOPMENT

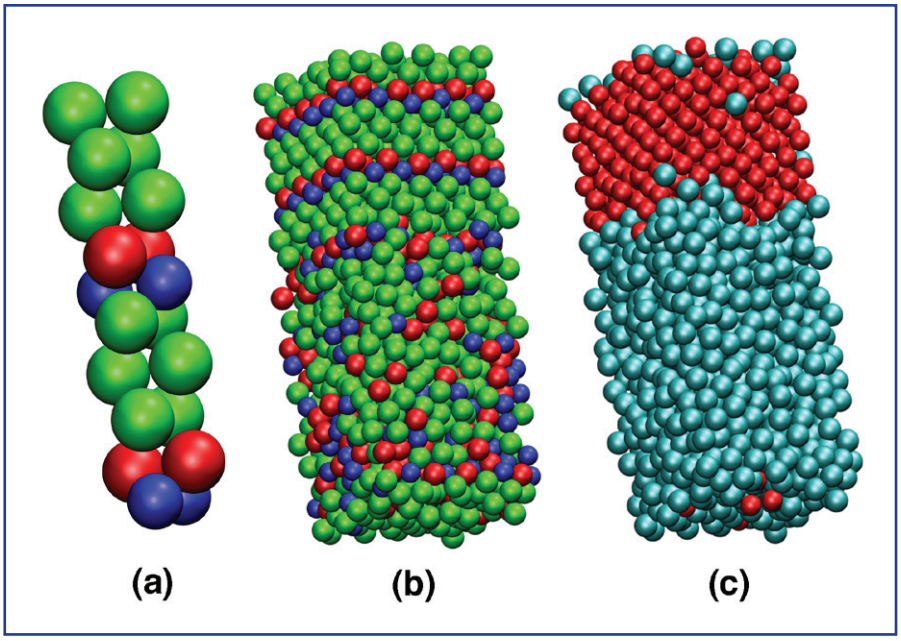

Figure 2: a) Two unit cells of the binary LJ system are shown. Species A is colored red in the AB CsCl phase and green in the A (FCC) phase. Species B is colored blue. Together, these two unit cells represent the smallest translatable unit for this crystal. (b) A two-thirds melted 5×5×6 crystal of binary LJ system. (c) The atoms of (b) have been re-labeled as crystalline (red) or non-crystalline (cyan). This figure was featured on the cover of the *Journal of Chemical Physics*, Vol. 131, Issue 7 (August 21st, 2009).

Significantly, the team was able to show that the previously published TTM+MD approach [3] leaks energy. The improved version was added to Sandia's massively parallel MD code, LAMMPS [4], and used for the simulations of radiation damage in single-component and binary Lennard-Jones (LJ) crystals [1].

The single-component face-centered-cubic (FCC) LJ crystals show remarkable resilience to radiation damage (Figure 1), whereas the binary glass-forming LJ crystal retained damage much more easily (Figure 2). For both of these LJ systems, a scan of TTM parameter space was performed to investigate how the electronic subsystem properties and its coupling with the atomic subsystem influenced material damage. A special shape-matching algorithm was used to identify damaged material.

In general, these models can be used to capture other high-energy events such as laser heating, sputtering, shock-induced melting, heterogeneous melting, and cascade simulations. Thus, Sandia will be able to perform increasingly improved simulations to the many critical processes that impact both materials and electronic components.

References

1. Phillips, C.L., and Crozier, P.S. (2009). An energy-conserving two-temperature model of radiation damage in single-component and binary Lennard-Jones crystals, *J. Chem. Phys.*, Vol. 131, Article No. 074701.
2. Greathouse, J.A., Crozier, P.S., Ismail, A.E., and Foiles, S.M. (2009). *The Effect of Electron-Ion Coupling on Radiation Damage Simulations of a Pyrochlore Waste Form*, SAND2009-6892. Sandia National Laboratories, Albuquerque, NM.
3. Duffy, D. M. and Rutherford, A. M. (2007). Including the effects of electronic stopping and electron-ion interactions in radiation damage simulations, *J. Phys.: Condens. Matter*, Vol. 19, Article No. 016207.
4. The TTM-MD module for LAMMPS is available for download as part of the LAMMPS MD package at http://lammps.sandia.gov. Specifically, see: http://lammps.sandia.gov/doc/fix_ttm.html

Toward Computational Atomic-Scale Design and the Predictive Engineering of Materials

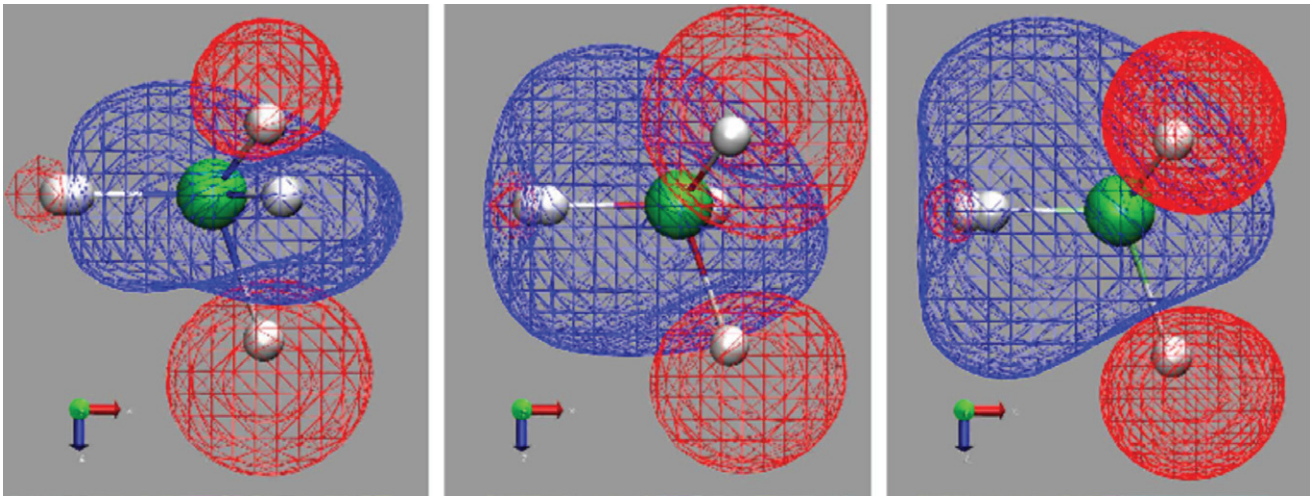

Figure 1: Differences in external potentials for superimposed compound pairs NH_3/CH_4, H_2O/CH_4, and HF/CH_4 (left to right). Blue and red represent positive and negative isovalue surfaces, respectively.

Researchers are exploring the purposeful design of compounds with optimized properties.

For more information:

Technical Contacts:
O. Anatole von Lilienfeld
505-284-8829
oavonli@sandia.gov

Science Matters Contact:
Alan Burns
505-844-9642
aburns@sandia.gov

Systematic approaches towards the virtual engineering of chemical composition, attempting to computationally identify compound candidates that meet sets of specific desired property requirements, is a worthwhile goal in general, and for pharmaceutical and materials research in particular. Ideally, quantitative structure property relationships (QSPR) can be identified, and used for numerical screening or within optimization algorithms. The eventual goal being, to answer the ``inverse'' question: under specified conditions, which compound will exhibit a certain desired property?

The concept of Chemical Compound Space (CCS) has recently received increased attention in the computational physical, chemical, biomolecular and atomistic materials sciences in the context of its exploration for the purposeful design of compounds with optimized properties. CCS, the combinatorial set that encompasses all stable chemical compounds, provides a rigorous framework in which to construct the mathematical tools for the development of physical chemistry-based direct and inverse QSPRs. One can view CCS as the high dimensional set populated by all the possible combinations (stoichiometries) and configurations (isomers) of elementary particles that make up electronic and nuclear densities. Due to the large cardinal number of CCS, simple enumeration is computationally prohibitive. For example, alkanes (a relatively simple class of molecules) with up to 80 carbon atoms are estimated to include more than 10^{28} topological isomers. Consequently, listing the corresponding molecular topologies becomes practically impossible, let alone attempts to screen. In general, the *de novo* design of interesting material is very likely to be tackled inefficiently by screening methods. This is not only because CCS is astronomically large but also because the chances to "stumble" across a "hit" decrease exponentially with the number of

material properties (if uncorrelated) that must be exhibited simultaneously.

This inefficient state of affairs has motivated the development of more "rational" first principles design methodologies that usually rely on electronic-structure methods because composition, and thereby chemical bonding, must be varied frequently and freely. In order to optimize electronic eigenvalues (ε) of materials (a central property relevant to photo-voltaic, battery, or catalysis applications) "alchemical" gradients in CCS have been developed that measure the response of ε to changes when the computational model of compound *i* is continuously transformed into the computational model of compound *j*, driven by an order parameter (λ). Such gradients could form the future basis for gradient-based optimization algorithms that generally offer drastically improved performance.

If both compounds have the same number of electrons, research at Sandia has shown that the gradient of their electronic potential energy (*E*) is the quantum mechanical expectation value of the difference of their corresponding Hamiltonians (*H*). Within the electronic structure method Density Functional Theory, this expectation value is tantamount to the integral over the product of electron density (*n*) and the difference in external potentials (*v*):

$$\frac{dE(\lambda)}{d\lambda} = \langle H_j - H_i \rangle_\lambda = \int d\mathbf{r} n_\lambda(\mathbf{r}) \cdot [v_j(\mathbf{r}) - v_i(\mathbf{r})]$$

Figure 1 features differences in external potentials for three exemplary isolated compound pairs: NH_3/CH_4, H_2O/CH_4, and HF/CH_4. Figure 2 illustrates the ε-property as a function of λ (symbols) and predictions of CH_4's ε-property made using gradients at NH_3, H_2O, or HF (solid arrows). These predictions deviate substantially from the ideal predictions (pink) that would be useful for gradient-based optimization algorithms. Based on an empirical scheme, corrected predictions have been developed that promise higher accuracy (dotted arrows). The next step will be to tie these gradients into gradient-based optimization algorithms of materials properties.

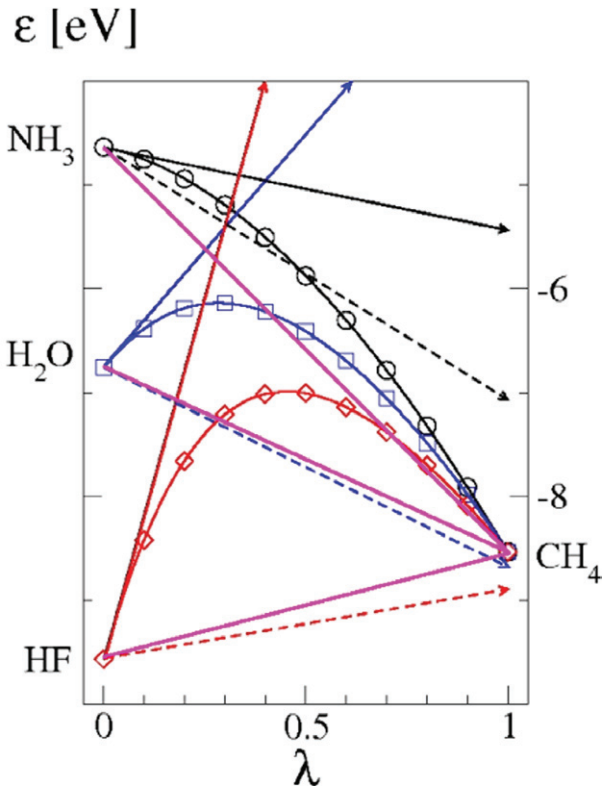

Figure 2: : ε-property as a function of λ (symbols), and predictions of CH_4's ε-property made using gradients at NH_3, H_2O, or HF (arrows). Pink lines correspond to perfect predictions.

Reference:

"Accurate ab initio energy gradients in chemical compound space" O. Anatole von Lilienfeld, *J. Chem. Phys.* **131** 164102 (2009)

Dynamics of Propagating Reaction Waves in Nanolaminate Foils

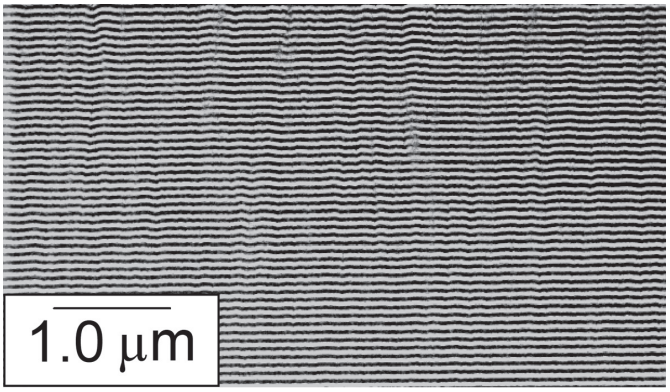

Figure 1: Cross-section, bright field transmission electron microscope image of an unreacted Ni/Ti nanolaminate foil. (Acknowledge: L. Brewer)

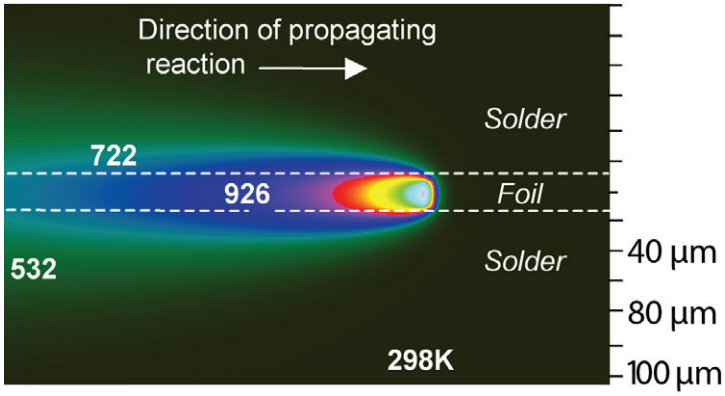

Figure 2: A simulated 'look' at a reaction front (shown in cross section) in a reactive Al/Pt nanolaminate constrained between two inert metals. Temperatures indicated are in degrees Kelvin.

The extreme temperatures of reaction generated by laminate metal foils may find broad application in materials joining processes

For more information:

Technical Contact:
David Adams
505-844-8317
dpadams@sandia.gov

Science Matters Contact:
Alan Burns
505-844-9642
aburns@sandia.gov

Reactive nanolaminate foils have recently garnered interest for alternative joining processes that require localized soldering or direct attachment. As shown in Figure 1, they consist of alternating layers of metallic films, such as nickel (Ni) and titanium (Ti), that are fabricated by sputter deposition in a vacuum environment. Individual reactant layer thicknesses are precisely controlled, typically in the range of 5-500 nm; total foil thicknesses vary from 5-100 µm, depending on the intended application. The finished foil is then applied to the surfaces that require joining. The chemical energy contained initially within a nanolaminate foil can be released as heat to melt and flow a neighboring filler material such as a gold-tin solder. By using only the heat evolved from a reactive nanolaminate for joining, there is virtually no thermal effect on neighboring temperature-sensitive devices or components, and minimal strain energy is developed in the assembly. For these reasons, exothermic nanolaminate joining processes have sparked interest in the microelectronics industry for lid seal, die attach and bonding sputter deposition targets[1].

Reactive nanolaminates are of scientific interest because they exhibit extreme temperature fluctuations that can result in far-from-equilibrium crystal structures. A simulation of a propagating reaction and its cross-sectional temperature profile is shown in Figure 2. Furthermore, reactive nanolaminates grown by vapor deposition are an ideal class of materials for evaluating how reaction dynamics depend on reactant layer spacing and composition. Although it is well-established that the ignition thresholds[2] and reaction speeds of exothermic nanolaminates are directly affected by their nanometer-scale periodicity (see Figure 3), little is known about the dynamics of propagating reaction waves and how these events affect the final state of a foil. Understanding the reaction dynamics is essential to the aforementioned applications, because the manner in which heat is released influences the

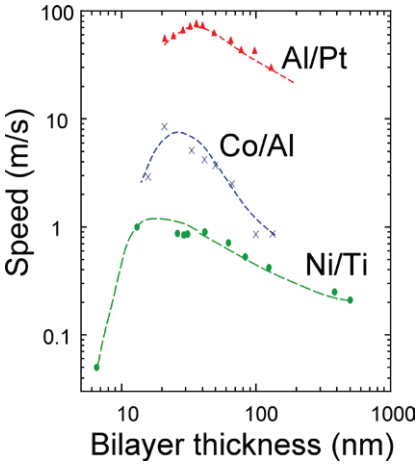

Figure 3: Plot of average propagation speed versus laminate periodicity for three exothermic material systems. Lines are guides to the eye.

microstructure, phase and surface morphology of the product foil and the structural integrity of a joined assembly.

Sandia researchers and their collaborators[3] have investigated the dynamics of high-temperature, self-propagating reactions in metal-metal nanolaminates. Using both fast optical and *in situ* transmission electron microscopy, they have probed the evolving reactions and have determined how the shape of a reaction front depends on multilayer design, stored chemical energy, environment, and foil thickness. High exothermicity systems ($\Delta H_o \approx$ -100 kJ/mol) generally exhibit a microscopically-uniform reaction front with rapid average propagation speeds as high as 100 m/s. Low exothermicity systems ($\Delta H_o \approx$ -50 kJ/mol) exhibit unstable propagation modes characterized by a non-uniform reaction front morphology and reduced speeds. Unstable modes result from a decoupling of the atomic diffusion and thermal waves associated with a reaction front. In Figure 4, the shape of an unstable reaction front in a cobalt/aluminum (Co/Al) nanolaminate is demonstrated. Here, in plan view, the atomic diffusion wave lags the thermal wave, resulting in a propagating reaction mode that is characterized by transverse reaction bands originating at the boundaries of a specimen or at the intersections of colliding fronts [4]. This behavior is called a "spin-like reaction."

The tendency to exhibit unstable spin-like behavior (versus stable modes) can have a direct effect on surface morphology and, in some cases, microstructure and phase formation. In Figure 5, scanning electron microscopy shows the surface morphology of a reacted Co/Al foil after it has cooled. In this case, a multi-periodic surface morphology developed as a result of spin-like propagating reaction waves with the wavelength of the final surface corresponding to the width of transverse propagating reaction bands.

Continued development of reactive nanolaminates for hermetic sealing and more broadly-applicable joining processes (potentially brazing) will benefit from an improved understanding of reaction dynamics, heat release rate and their effects on final foil properties including microstructure and morphology.

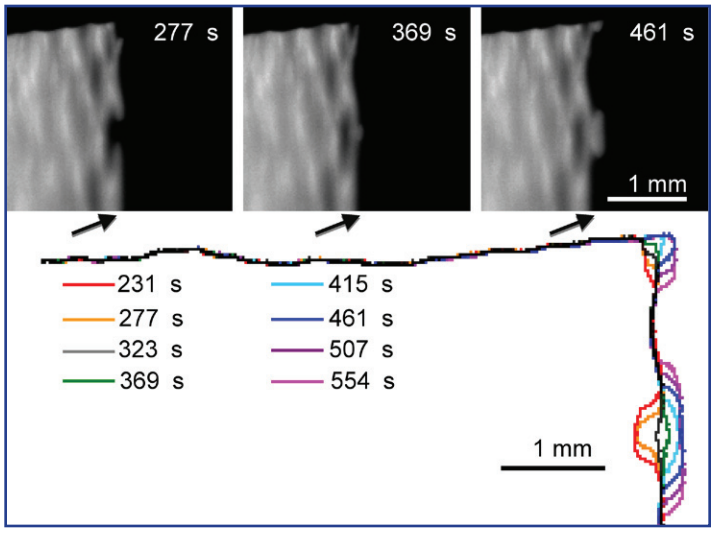

Figure 4: Time evolution of spin-like reaction waves in Co/Al. The three images show the surface of a reacting foil in plan view with reacted (hot) material appearing bright. Changes over time are observed at the reaction front (arrows). Spin-like behavior is evidenced by the propagation of reaction bands that move transverse to the net direction of the reaction wave (left-to-right). The color diagram depicts how colliding bands advance a reaction front a given distance (~ 0.25 mm), with continued reaction waves moving in opposite directions.

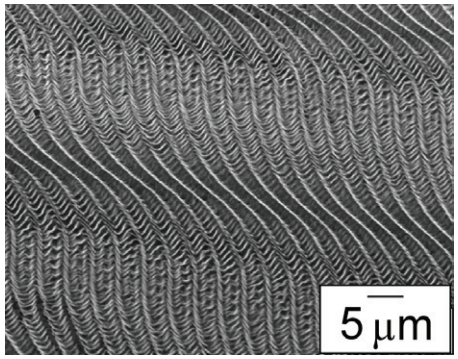

Figure 5: Scanning electron micrograph of a reacted CoAl foil showing a rippled surface structure that is a direct result of propagating bands.

References

1. J. Wang, E. Besnoin, O.M. Knio, and T.P. Weihs: Investigating the effect of applied pressure on reactive multilayer foil joining. *Acta Mater.* **52**, 5265 (2004).
2. Y.N. Picard, J.P. McDonald, T.A. Friedmann, S.M. Yalisove and D.P. Adams: Nanosecond laser induced ignition thresholds and reaction velocities of energetic bimetallic nanolaminates, *Appl. Phys. Lett.* **93**, 104104 (2008).
3. A collaboration with T. Lagrange and G. Campbell (Lawrence Livermore National Laboratories).
4. J.P. McDonald, V. Carter Hodges, E.D. Jones Jr. and D.P. Adams: Direct observation of spin-like reaction fronts in planar energetic multilayer foils, *Appl. Phys. Lett.* **94**, 034102 (2009).

Small Particles for Solving Big Problems: Using MOFs for Nanoparticle Synthesis

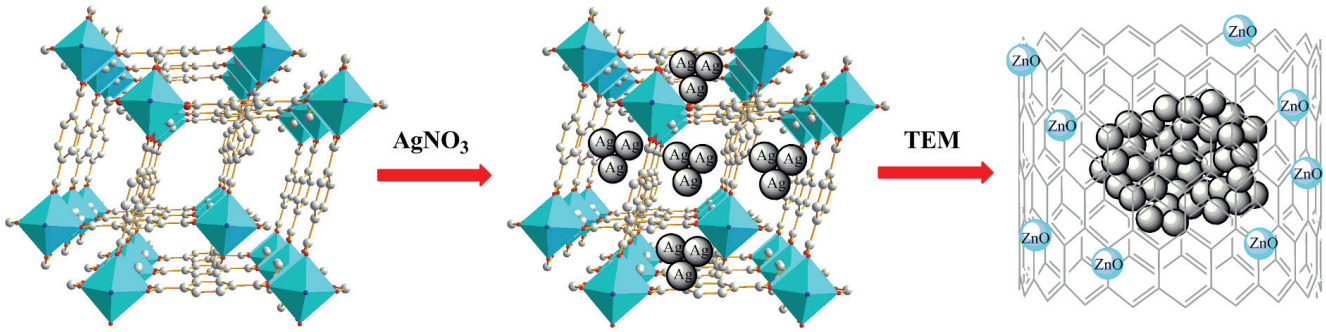

Figure 1: Using MOFs to create nanoclusters. *Left*: empty MOF structure (blue: octahedrally-coordinated zinc atoms; red: oxygen; blue: nitrogen; gray: carbon); *Middle*: silver-infiltrated MOF following *in-situ* reduction to create nanoclusters stabilized by the framework. *Right*: subsequent exposure to a high energy TEM beam breaks down the MOF and allows Ag agglomeration.

Versatile nanoporous materials allow new approaches to both nanoparticle synthesis and hydrogen storage

For more information:

Technical Contact:
Mark Allendorf
925-294-2895
mdallen@sandia.gov

Science Matters Contact:
Alan Burns
505-844-9642
aburns@sandia.gov

Shrinking materials to nanoscale dimensions can have interesting and potentially useful consequences. For example, gold particles in the 10–100 nm size range can emit bright light and be used to track individual molecules in biological systems. Even smaller particles are being investigated for their potential as "super catalysts." On a commercial scale, silver nanoparticles have been incorporated into washing machines because of their antibacterial properties. However, both the synthesis and the characterization of nanomaterials present major scientific and engineering challenges, particularly when their dimensions are smaller than 10 nm.

Sandia is developing novel nanoporous materials known as metal-organic frameworks (MOFs) as templates for nanoparticles. A typical MOF (Figure 1) consists of positively-charged metal atoms such as Zn^{+2} linked by negatively-charged organic groups such as carboxylates (CO_2^-), yielding a rigid, open framework that can accommodate guest atoms and molecules. The pore size and chemical properties of MOFs can be tailored for applications ranging from gas storage to sensing. The interior dimensions of MOF pores range from less than 1 nm to about 5 nm and have enclosed pores or one-dimensional open channels. Two examples are given here that dem-onstrate the extremely versatile MOF platform for both probing unusual effects in nanoscale particles, and to also serve as a novel synthetic tool for creating particles of controlled size and shape.

The first example concerns the creation of silver nanoparticles within MOF templates (see Figure 1). MOF pores infiltrated with solutions of silver nitrate and ethanol generate nanoparticles because ethanol reduces the Ag^{+1} ions to uncharged silver (Ag^0), creating silver particles so small they cannot be seen even by transmission electron microscopy (TEM). The smallest particles have only three atoms (Ag_3) and can be clearly identified by their magnetic properties; the largest particles have approximately 20 atoms, which are about 0.7 nm in diameter. The particles are stabilized by oxygen-containing groups

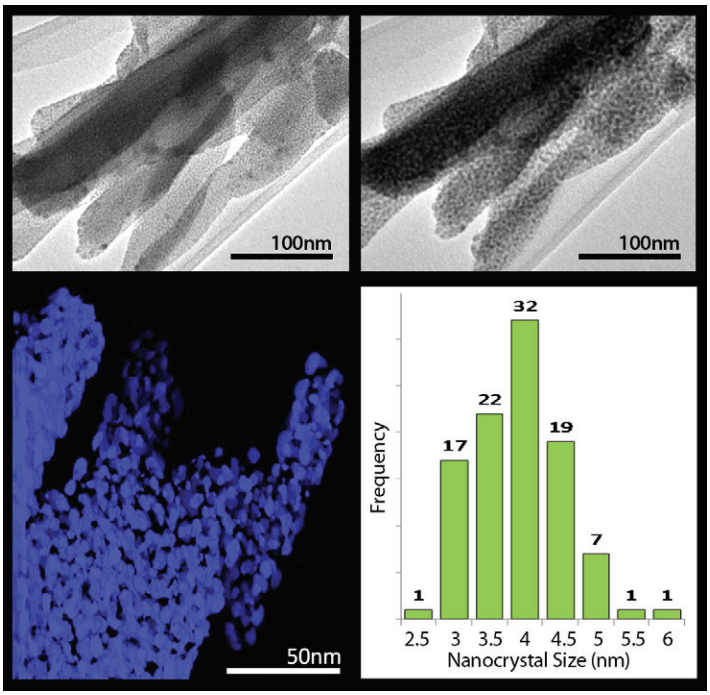

Figure 2: Before and after images of Ag@MOF. *Top left*: Image of Ag@MOF before significant electron beam damage. *Top right*: Image of Ag@MOF after 1 minute electron beam exposure, showing formation of larger silver particles (small black dots). *Bottom left*: tomographic image showing silver nanoparticles throughout a MOF crystal. *Bottom right*: size distribution of TEM-synthesized Ag nanoparticles, where the average size is 3.9 ± 0.65 nm.

within the MOF structure that also prevent particle diffusion through the pore openings of the template. However, they are still accessible to solvent and other small molecules, thus creating a platform for probing their chemistry. Larger particles ranging in size from just a few nanometers to tens of nanometers can be formed by decomposing the template with the TEM electron beam or by heating the sample to 250-310 °C (Figure 1 right, and Figure 2). As shown in Figure 2, the size distribution can be quite narrow. Also, the electron beam synthetic method has been generalized to create nanoparticles from the MOF templates alone, with success in making bare copper and indium nanoparticles, as well as zinc oxide nanoparticles. These results demonstrate the versatility of the "metal@MOF" platform, which has significant advantages for nanoparticle synthesis. For example, MOF templates avoid the use of bulky capping molecules needed to prevent agglomeration in solution-based nanoparticle synthesis (the capping molecules can inhibit nanoparticle utility).

The second example concerns the use of MOF templates to create nanoparticles of metal hydrides for hydrogen storage. Recent theory and experiment suggest that shrinking metal hydrides to the nanoscale enables tuning of hydrogen desorption thermodynamics and kinetics, potentially allowing hydrides that are normally irreversible in the bulk phase to be used for vehicular hydrogen storage. Sandia is systematically probing the effects of size and pore environment on metal hydride H_2 desorption kinetics using MOF templates, which are an attractive alternative to materials such as aerogels and mesoporous silica that have a distribution of pore sizes. Experiments show that MOFs are stable hosts for several metal hydrides and that nanoclusters on the scale of MOF pores can be synthesized. These materials exhibit reduced H_2 desorption temperatures and accelerated desorption kinetics (Figure 3). The results provide a scientific basis for designing nanoscale hydrides with desorption rates appropriate for hydrogen storage applications.

These examples illustrate the versatility of MOFs to serve as templates for a wide variety of nanoparticles and to probe their properties. Sandia's research is now aimed at a better understanding of the underlying mechanisms for particle formation, growth, and stabilization, so that they can be employed in practical applications.

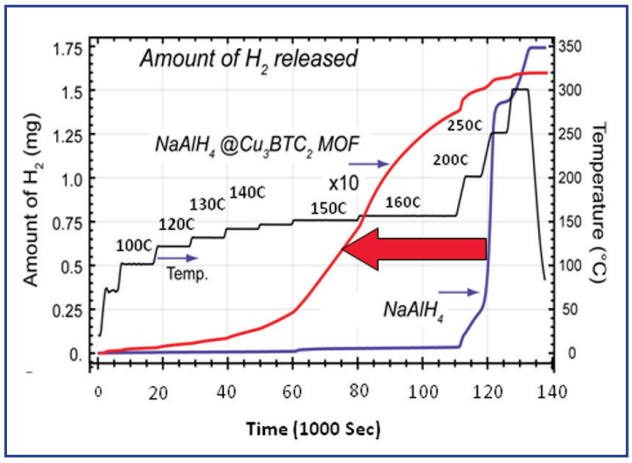

Figure 3: Amount of H_2 released from MOF infiltrated with $NaAlH_4$ (red line) compared with bulk-phase $NaAlH_4$ (blue line). The stepped black line in the plot indicates the temperature profile used to heat the samples.

References:

R. K. Bhakta, J. L. Herberg, B. Jacobs, A. Highley, R. Behrens, Jr., N. W. Ockwig, J. A. Greathouse, and M. D. Allendorf "Metal-Organic Frameworks As Templates for Nanoscale NaAlH4," *J. Amer. Chem. Soc.* **131** (2009), 13198

R. J. T. Houk, B. W. Jacobs, F. El Gabaly, N. N. Chang, A. A. Talin, D. D. Graham, S. D. House, I. M. Robertson, and M. D. Allendorf "Silver Cluster Formation, Dynamics, and Chemistry in Metal-Organic Frameworks," *Nano Lett.* **9** (2009), 3413.

Growth Mechanisms that Control InGaN Step Morphology

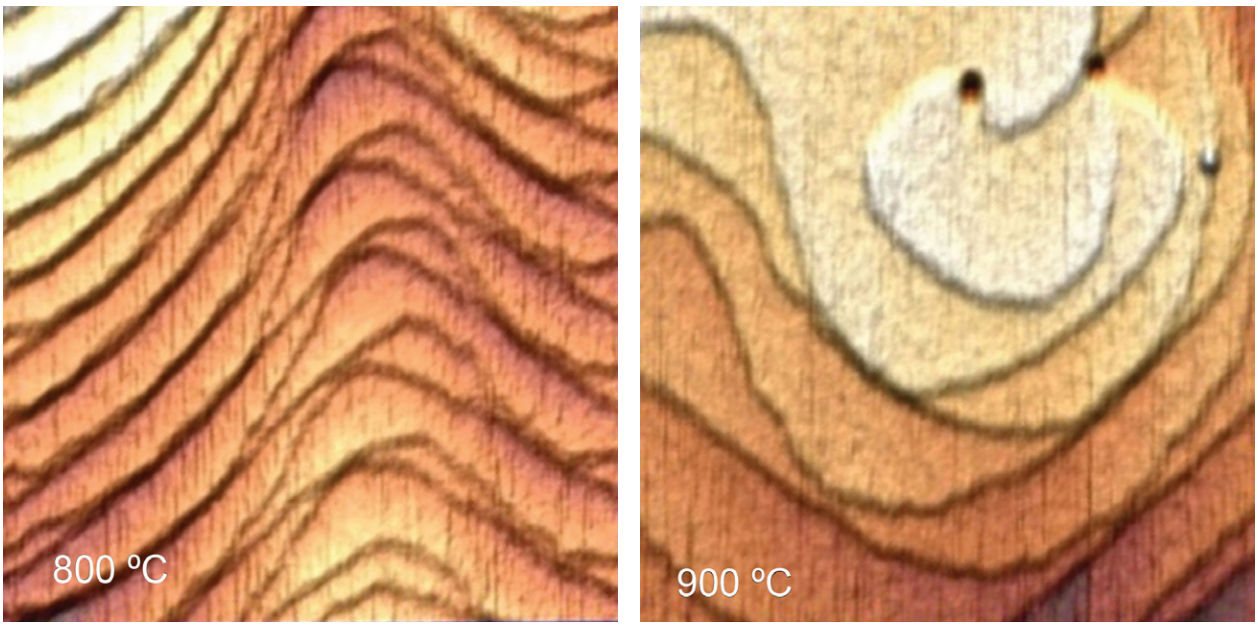

Figure 1: Atomic force microscopy images (1x1 μm) of InGaN/GaN surface morphologies when the GaN barriers are grown at T=800 °C (left) and T=900 °C (right).

Emission intensity from quantum well devices may be linked to morphology acquired during thin film growth

For more information:

Technical Contact:
Daniel Koleske
505-284-4531
ddkoles@sandia.gov

Science Matters Contact:
Alan Burns
505-844-9642
aburns@sandia.gov

In the U.S., more than 30% of all generated electricity is being used for lights in buildings and elsewhere. This is because traditional incandescent and fluorescent bulbs are not very efficient in converting electrical power into visible light. For this compelling reason, researchers worldwide are developing much more energy-efficient light emitting diodes (LEDs). Indium gallium nitride (InGaN) is an important compound semiconductor material that is being used to make bright, white-light LEDs. However, unlike other LED semiconductors, it typically contains a large number of defects when grown on flat sapphire substrates. Several theories have been proposed to explain how InGaN LEDs are able to operate despite the large defect density. While important details of these theories vary, the general consensus is that the process of electrical carrier localization allows the carriers to produce useful light; otherwise the carriers would migrate to defect sites where they undergo dark recombination and produce no light. Recently, Sandia has explored InGaN surface morphology in order to study how InGaN quantum well (QW) structures can be structurally tailored to possibly enhance localization and thereby improve LED brightness.

In one study, Sandia researchers grew 5-period InGaN quantum wells (QWs), which is the light-producing region of the LEDs, sandwiched between GaN barrier layers. The growth temperature can have a profound influence on the surface morphology of these materials. Examples of the temperature dependence are shown in Figure 1, where two otherwise identical QW structures were grown at the GaN barrier temperatures of 800 °C (left image) and 900 °C (right image). Comparison of these two images shows a difference in the step height and frequency morphology. For the film with GaN barriers grown at 900 °C, the steps heights are predominantly monolayer

Sandia National Laboratories

National Nuclear Security Administration

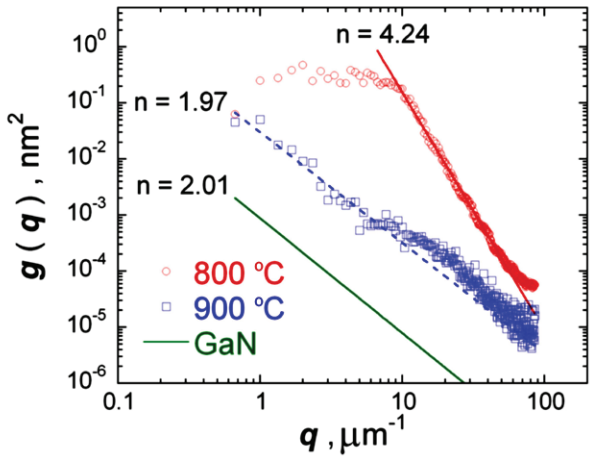

Figure 2: Calculated power spectral density, *g*, plotted as a function of the reciprocal length,*q*, for QWs where the GaN barrier is grown at either 800 °C (red) or 900 °C (blue). The *g*(*q*) for a high temperature grown GaN template is shown in green.

(c/2 where c is the c-axis lattice constant) in height; while for the film with barriers grown at 800 ºC, there is an increase in the number of double-layer steps. The increase in the double-layer step frequency also means that the QW film with 800 ºC grown barriers is "rougher" than the QW film with 900 ºC grown barriers.

More advanced analysis of the images shown in Figure 1 can reveal how the surface roughness varies with distance and what mechanism is responsible for producing the observed morphology. For this analysis, the height-height correlation function or power spectral density, *g*, is calculated as a function of the reciprocal length scale, *q*. The root mean square roughness of the surface is obtained by taking the square-root of the sum of g(q) values over all q. A plot of g(q) vs. *q* is shown in Figure 2 for films with GaN barriers grown at 800 ºC (red) and at 900 ºC (blue), along with that of the blank, starting GaN template (green line). Notice that *g*(*q*) for the 800 ºC film are larger than those for the 900 ºC film, again indicating that the 800 ºC film is rougher.

Surface "smoothing" mechanisms during film growth can be discerned from the *g*(*q*) power dependence, n, following the work of Conyers Herring in 1950 [1]. For the 800 ºC QW sample, *n*=4.24 (red line); while for the 900 ºC QW sample, *n*=1.97 (blue line). For comparison, the underlying high-temperature-grown GaN templates (green line) has *n*~2. Herring showed that *n* values near 2 are consistent with a smoothing mechanism involving evaporation and recondensation of atoms on the surface. This leads to smoother surfaces with longer length scale features (1-10 µm). While *n* values near 4 are consistent with a smoothing mechanism involving surface diffusion [1], resulting in rougher surfaces with shorter length scale features (10-100 nm). The two smoothing mechanisms are summarized in Figure 3.

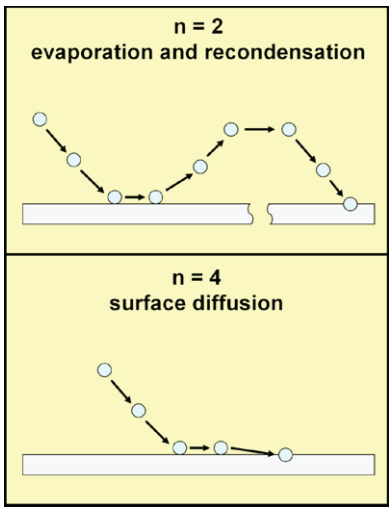

Figure 3: Depiction of the two surface smoothing mechanisms for InGaN/GaN at different GaN barrier growth temperatures. (Top) Evaporation and recondensation mechanism that occurs when growth T=900 °C. This leads to smoother surfaces with longer scale features (1-10 µm). (Bottom) Surface diffusion mechanism at growth T=800 °C. This leads to rougher surfaces with shorter scale features (10-100 nm).

Finally, photoluminescence (PL) measurements reveal brighter emission from multiple quantum wells (MQWs) with barriers grown at 800 ºC compared to MQWs with barriers grown at 900 ºC, as seen in Figure 4. X-ray diffraction studies of these two samples find similar indium concentrations (~20%) and QW thicknesses for both MQWs, suggesting that the difference in emission intensity may be due to enhanced localization in QWs grown on the more textured 800 ºC barrier layers.

Our work provides evidence that changes in growth mechanisms can be used to control InGaN/GaN MQW morphology; moreover, the morphology may be linked to emission efficiency. However, the causal link between the MQW growth morphology and PL emission intensity awaits further study.

Reference

1. C. Herring, *J. Appl. Phys.* **21**, 301 (1950).

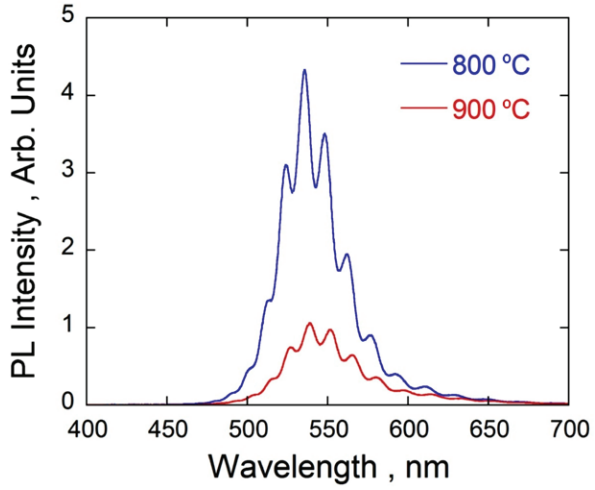

Figure 4: PL intensity for the two green light emitting MQWs shown in Figure 1 with GaN barrier temperatures of 800 ºC and 900 ºC.

Developing Nanoscience Tools for Li-ion Battery Research

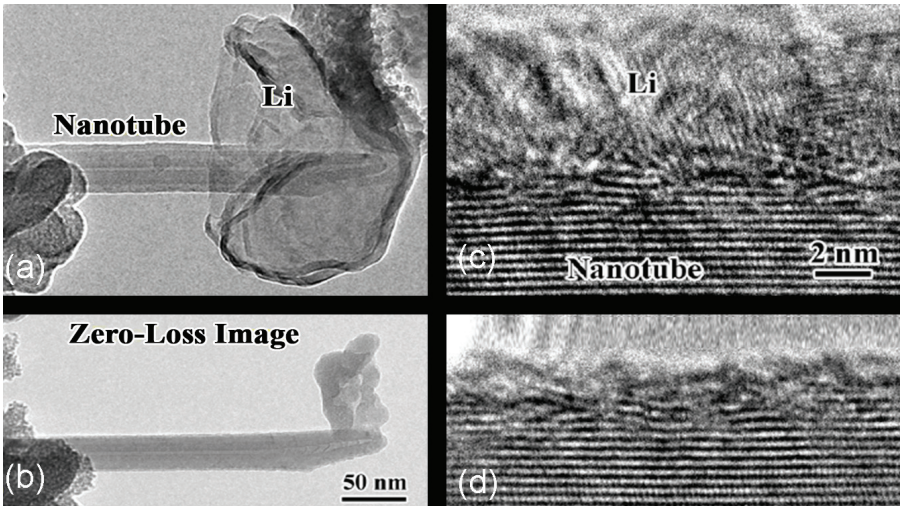

Figure 1: HRTEM images of the solid-state reaction between Li metal and a multi-wall carbon nanotube (MWCNT). (a) A Li particle in contact with the MWCNT reacts by diffusion and insertion between the walls of the MWCNT in approximately one minute (b). This process is imaged with atomic resolution near the start of contact (c) and after reaction completion, (d). An expansion of the inter-wall spacing is observed in (d).

Significant improvements in battery performance will require detailed, nanoscale studies of electrochemical materials

For more information:

Technical Contact:
John Sullivan
505-845-9496
jpsulli@sandia.gov

Science Matters Contact:
Alan Burns
505-844-9642
aburns@sandia.gov

In order to meet our nation's goals for energy efficiency and green energy production, major improvements are needed in electrical energy storage. The rechargeable Li-ion battery is widely recognized as offering the best energy-to-weight performance (an important metric in portable applications). The success of Li-ion batteries is due to years of careful development of the anodes, cathodes, and separator materials. However, in order to meet broad application goals requiring a factor of two increase in performance, these material systems and architectures will need to change significantly.

The research challenge is that the materials that are currently used, as well as those that are proposed, are often a mixture of multiple phases of nanoscale to microscale dimension, and it is exceedingly difficult to directly measure the structure and electrochemical performance at these length scales. Thus Sandia is developing tools and capabilities to measure the structural changes and electrochemical behavior of Li-ion battery materials during active charge-discharge cycling down to the single-particle level and with atomic to nanoscale spatial resolution. To achieve this, researchers have developed microfabricated platforms to isolate individual nanoparticle battery components and permit their characterization during electrochemical cycling inside a high-resolution transmission electron microscope (HRTEM).

Sandia has developed two approaches to perform electrochemistry inside the high vacuum of the HRTEM: (1) "open cells" using ionic liquid electrolytes, and (2) "sealed cells" that are created using microelectromechanical systems (MEMS) processed at the MESA (Microsystems and Engineering Sciences Applications) Facility. As a first step towards "open cell" electrochemistry inside a HRTEM, researchers have examined the sequence of lithium insertion in multi-wall carbon nanotubes (MWCNT) via solid-state reaction (sans electrolyte), as shown in Figure 1a-d. A particle of lithium metal was placed in

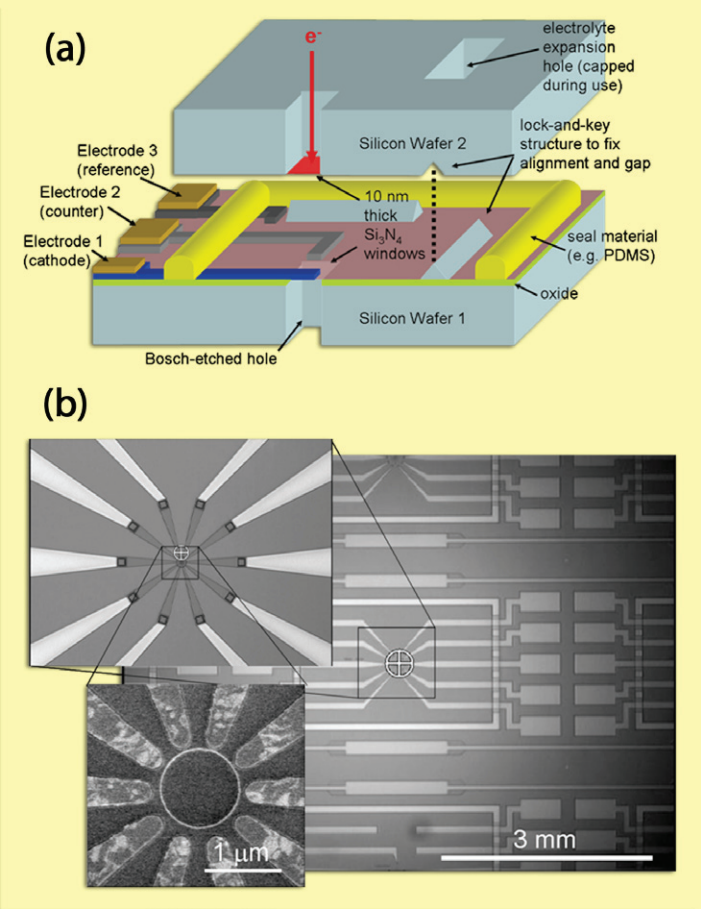

Figure 2: (a) A schematic of the sealed electrochemistry cell for HRTEM studies of battery electrochemical processes. The platform is constructed using a flip-chip approach combing two MEMS chips that encapsulate a thin layer of electrolyte between electron-transparent windows. (b) Images of the lower chip of the platform showing the dense array of closely-spaced electrodes. This electrode geometry enables DEP of nanoscale battery materials.

contact with a MWCNT using a nanomanipulator inside the HRTEM (Figure 1a). In approximately one minute of imaging, the lithium reacts with carbon and intercalates between the walls of the MWCNT (Figure 1b). This process is followed with atomic resolution (Figures 1c and 1d), where an increase in the interwall spacing of the nanotube is observed, consistent with lithium intercalation. This experiment is currently being repeated with an ionic liquid electrolyte separating the lithium metal and MWCNT, permitting liquid electrochemical studies inside the HRTEM.

Researchers are also interested in imaging the formation process and spatial distribution of the solid-electrolyte-interphase, a reaction product between the battery electrodes and ethylene carbonate-based electrolytes. In order to use the electrolyte inside the vacuum environment of TEM, Sandia applied MEMS technology to develop sealed electrochemical cells (Figure 2). The sealed platform is created by bonding two chips using a flip-chip approach, with the bottom chip containing a dense array of buried electrical interconnects that permit electrical contact to battery materials. Figure 2(b) shows the bottom chip and a close-up of the electrical interconnect structure designed to permit the assembly, via dielectrophoresis (DEP), of nanoparticles and nanowires across a narrow electron-transparent aperture. In DEP, AC electric fields enable the placement of individual nanoparticles and nanowires, initially suspended in solution, across the narrow electrode gaps. Figure 3(a) shows electron microscopy images of DEP-assembled nanostructures across gaps. This technique thus isolates individual nanoscale battery materials and enables studies of their electrochemical performance.

This work is creating new tools for understanding the electrochemical processes of nanoscale battery materials during real-time operation. This is an important capability that will aid in understanding the degradation processes in existing Li-ion batteries, as well as aiding in the development of new, higher performance battery materials. Examples of these new materials include conversion anode materials, based on silicon, tin oxide, and iron oxide, and new high voltage cathode materials, such as $LiNiPO_4$. Without this new characterization capability, much of the battery development will occur without understanding the mechanisms, and this could lead to unexpected pitfalls or missed opportunities for improvement. Ultimately, the development of a high performance energy storage technology will enable practical electric vehicles, miniaturized remote sensors, and more practical green energy technologies by leveling the short-frequency variations in power production.

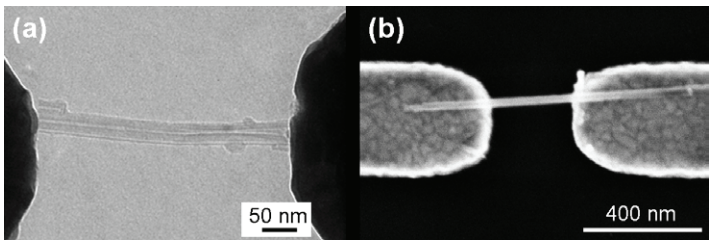

Figure 3: Examples of using DEP to assemble battery electrode materials. (a) HRTEM images of a multi-wall carbon nanotube placed across a silicon nitride electron-transparent membrane. (b) A SEM image of a MnO_2 nanowire spanning an electrode gap. When reacted with Li, MnO_2 is a common Li-ion cathode material.

Materials Science and Technology
Materials Characterization

In-Situ Neutron Diffraction of Li-Ion Batteries

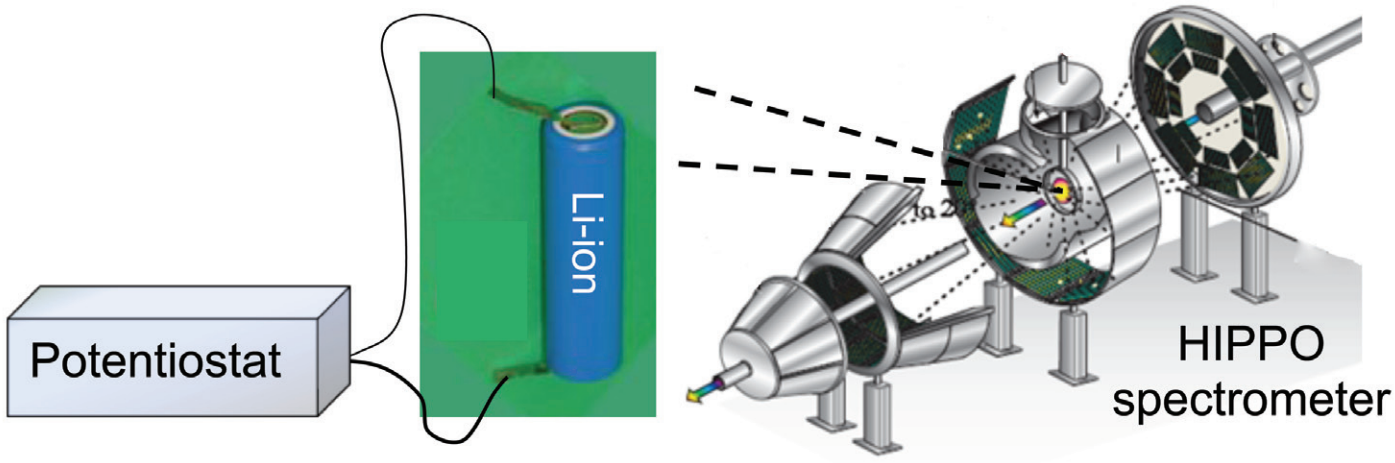

Figure 1: A standard cylindrical 18650-type Li-ion battery (LPF-1350, 2.5 Ah) was electroded to a potentiostat and cycled *in-situ* within the HIPPO neutron spectrometer at LANSCE in Los Alamos National Laboratory.

Time dependent materials analysis of charge/ discharge cycles will lead to improved electrical energy storage

For more information:

Technical Contact:
Mark A. Rodriguez
505-844-3583
marodri@sandia.gov

Science Matters Contact:
Alan Burns
505-844-9642
aburns@sandia.gov

In an era where electrical energy storage is becoming increasingly important, the understanding of electrochemical reactions in batteries is crucial. A science-based approach to understanding these reactions can lead to breakthroughs in battery capacity and performance. As a means of energy storage, batteries will need significant improvement in order to support the continually increasing demands of electric vehicles as well as portable electronics.

Sandia has been developing protocols that allow for diagnosis of electrochemical cell reactions "*in-situ*," that is, methods for monitoring a battery while it is undergoing charging and discharging. Typical materials science diagnostic techniques are not usually designed to accommodate this approach. Instead, a charge-discharge experiment would be performed on many batteries, each run to a given state-of-charge (SOC), followed by disassembly. The disassembled battery parts would be investigated in what is often termed a "post-mortem" analysis. However, such analyses do not always reflect the dynamic behavior of a battery system. Dynamic behavior is best obtained by the *in-situ* method.

In-situ measurements can be quite challenging. First of all, one must be able to collect data rapidly in order to capture changes while they are occurring. Another complication often arises from overlapping data. A dataset (e.g., a diffraction pattern) usually contains information from many different parts of a battery (anode, cathode, separator, electrolyte, external casing, etc). One must be able to sift through the results to isolate the signal associated with battery performance from signal that is irrelevant (and therefore unwanted). This is often so difficult that such attempts are abandoned in favor of post-mortem work. Early on, Sandia employed in-situ X-ray diffraction (XRD) analysis and has been able to overcome signal extraction issues by the use of multivariate analysis (MVA) techniques[1]. However, the XRD experiments required a specially-designed "coffee-bag" battery, since

Sandia National Laboratories

LDRD LABORATORY DIRECTED RESEARCH & DEVELOPMENT

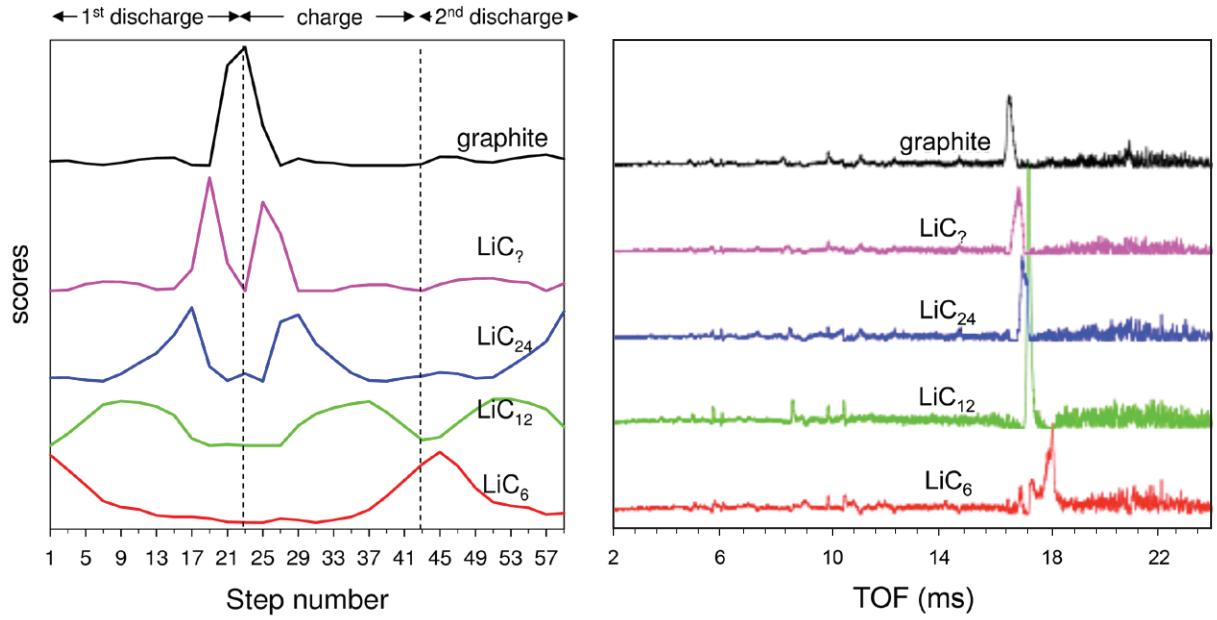

Figure 2: (*Left*) MVA scores with step number of neutron scattering analysis during Li-ion battery discharging and charging cycles. (*Right*) MVA-derived neutron diffraction histogram components from corresponding MVA analysis.

the X-ray beam cannot penetrate the outside containers of typical commercial batteries[1].

The problem of the outer packaging was solved by the use of highly penetrating neutron beams. Recent development of a neutron time-of-flight powder diffractometer called HIPPO (for High-Pressure-Preferred Orientation) at the Los Alamos Neutron Science Center (LANSCE) provides both a neutron scattering capability, along with sufficiently fast data collection for monitoring of the electrochemical behavior of a commercial battery. Sandia researchers and their Los Alamos collaborators chose a standard 18650 cylindrical Li-ion battery for their experiment (see Figure 1). A fully-charged battery was placed in the spectrometer and neutron diffraction data were collected during electrochemical cycling. By employing the use of MVA, the researchers were able to screen out noise and unwanted signal to reveal information about the ongoing chemical changes occurring in the cell. The cell was discharged, recharged, and discharged again.

Figure 2 shows the results for the anode behavior, with isolated component histograms from time-of-flight neutron diffraction (right side of figure) along with their corresponding scores (left). The histograms show strong peaks that are characteristic of lithium carbide (LiC_x) compounds (where x = 6, 12, etc). The neutron scattering scores are output from MVA, and can be thought of as proportional to concentration. The x-axis for the scores plot represents the step number and refers to the SOC of the battery at the time of measurement. These steps were roughly 10% of the battery's capacity. As one can see from Figure 2 (e.g., steps 1-23 in the first discharge), the various phases occur stepwise starting with LiC_6 at full charge followed by LiC_{12}, LiC_{24} and concluding with graphite devoid of Li upon complete discharge. This stepwise process, or "staging," is known to occur in graphitic Li-ion anodes[2]. What has not been documented is an additional phase (labeled $LiC_?$) that may be a possible LiC_{48} compound according to the component data (Figure 2 right); the new phase appears to be stable just before complete discharge. This new phase, precipitated from the multivariate analysis, has typically eluded detection. Likewise, additional analysis (not shown) successfully measured the simultaneous and complimentary reaction of $FePO_4$ to $LiFePO_4$ in the cathode of the battery.

The combination of *in-situ* analysis with the powerful MVA techniques shows promise for the dynamical diagnosis of functioning electrochemical cells, and should greatly enhance the understanding of batteries as entire systems. Future work will explore failure mechanisms of batteries and obtain heretofore overlooked subtleties regarding battery function that may be crucial in battery advancement.

References:

1. Rodriguez, M. A., Keenan, M. R., & Nagasubramanian, G. (**2007**). "*In situ* X-ray diffraction analysis of $(CF_x)_n$ batteries: signal extraction by multivariate analysis," *J. Appl. Cryst.*, **40**, 1097-1104.
2. Billaud, D., McRae, E. & Herold, A. (**1979**). "Synthesis and Electrical Resistivity of Lithium-Pyrographite Intercalation Compounds (Stages I, II, and III)," *Mat. Res. Bull.*, **14**, 857-864.

Materials Science and Technology
Applied Polymer Science

High-Char Foams for Abnormal Thermal Environmental Protection

Figure 1: A foam pillar transformed into a solid char with structural properties.

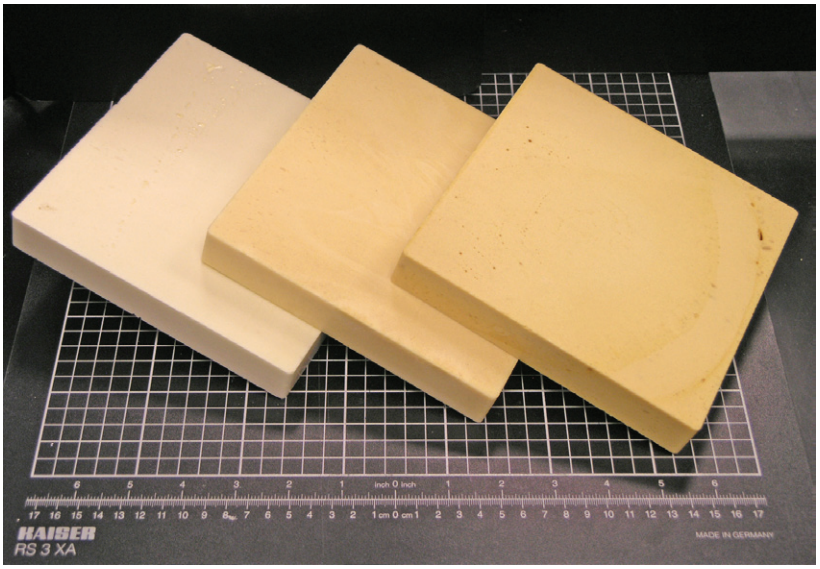

Figure 2: Examples of high char foam blocks ranging in density from 6 to 20 pounds per cubic foot.

Sandia develops novel packaging foams with previously inaccessible performance characteristics

For more information:

Technical Contacts:
Matthew Celina
505-845-3551
mccelin@sandia.gov

James Aubert
505-844-4481
jhauber@sandia.gov

Science Matters Contact:
Alan Burns
505-844-9642
aburns@sandia.gov

Many customized engineering systems developed at Sandia require sophisticated packaging to protect them from vibrational shock environments, thermal gradients, radiation exposures or particulate contamination. Systems requiring protection include sensitive electronic parts (microchips, electronic circuit boards), integrated satellites, and weapon system components. Packaging materials such as foams, conformal coatings, encapsulants and potting materials have one key feature in common - they involve the curing of reactive resins (their chemical building blocks), into a solid material with pre-defined properties. Thus, in many cases, the packaging materials share attributes no different than those found in common household epoxies, curable adhesives, or spray-on-demand foams.

Nearly all of the commercially available resins that are precursors for foam materials are relatively sensitive to pyrolytic decomposition at elevated temperatures, leading to mostly gaseous and liquid residues with minimal solid char formation. Thus exposure of packaged system components to abnormally high temperatures would result in unpredictable decomposition and poor solid, structural protection. With the ongoing emphasis in weapons engineering on surety innovation and predictable performance under abnormal environmental conditions, the high temperature behavior of encapsulation foams is a critical factor controlling the time-dependent behavior of thermal shielding and heat transfer. As long as a foam is capable of retaining its dimensions and shape by forming high amounts of solid black char residues (see Figure 1), then systems modeling is seen as a viable option to predict the condition of the protected internal components. Knowing precisely what thermal exposure may lead to is very important to better assess risk scenarios.

A Sandia research team has succeeded in developing a novel protective foam material that becomes 55% carbon char at 800°C (Figures 1 and 2). Unlike previously published materials, it does not rely on inorganic fillers that may introduce unwanted heavier elements or a higher viscosity that may lead to difficulties during foam processing. Instead, it is a hybrid material that uses a combination of an intrinsically high-char-forming cyanate ester resin (a customized resin precursor used in printed circuit boards and specialized composites), a high-char-yielding epoxy resin, a polymeric isocyanate resin for foaming and curing commonly used in polyurethane foams, and some additives for extra crosslinking and cure catalysis. There were several key steps in the development. These were recognizing the individual resin features, blending them into a synergistic material, understanding the competing cure reaction demands, and finally triggering specific cure kinetics with the help of suitable catalysts. In addition, the application of infrared spectroscopy (Figure 3) has enabled in-depth characterization of the cure reactions and resin interactions. The final product is a unique material that foams, solidifies and chars as required.

As with all reactive polymer foams, the foaming occurs in parallel with cure reactions. Liquid resins will transition into a solid material as the foam expands due to the significant exothermicity of the underlying crosslinking chemistry. Temperature control in the foam interior and reliable cure kinetics is absolutely critical to prevent overheating of larger foam blocks (Figure 2) and to establish a suitable framework for successful resin mixing and processing. A significant amount of work was devoted towards understanding individual reactions and mixing aspects of the foam system.

In terms of thermal expansion, glass transition temperature, and mechanical properties such as compression strength and modulus, the high char foam is as tough and attractive as other foams for structural and encapsulation purposes. Thus Sandia's first generation of this material is an excellent example of how applied polymer science can deliver a novel material for niche applications with previously inaccessible performance characteristics.

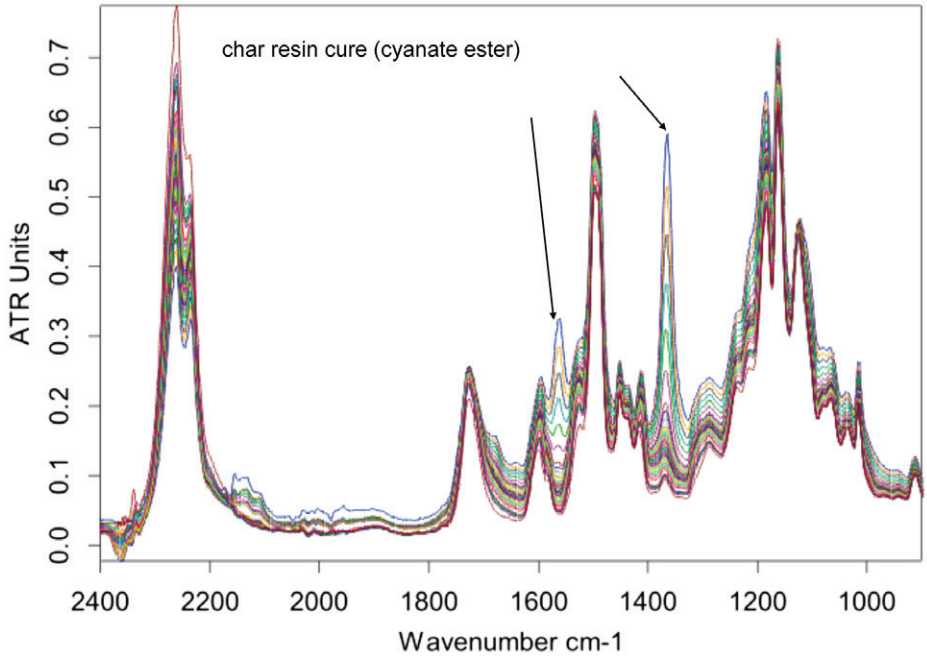

Figure 3: Time-dependent infrared spectroscopy provides information on the nature and timing of individual cure reactions (ATR = Attenuated total reflection). Cyanate ester reactions have specific spectral signatures and peak evolution (arrows) as a function of time.

Long-Wave Infrared Optical Cross Section Measurements of Biological Warfare Agents

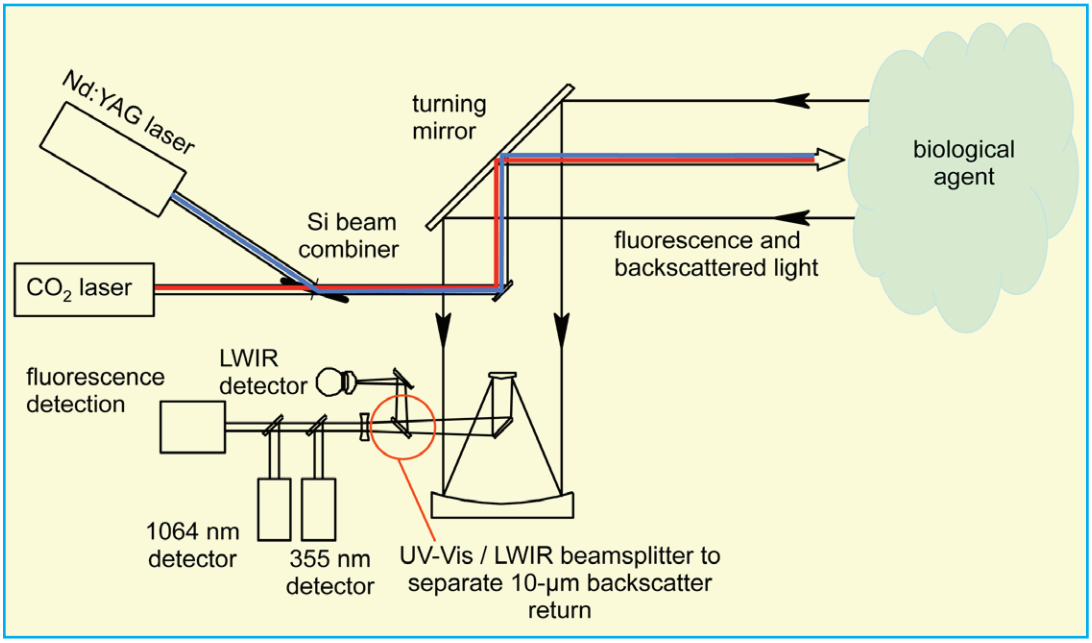

Figure 1: Schematic diagram of the new multi-wavelength range-resolved LIDAR to detect biological warfare aerosol agents.

A new multi-wavelength, range-resolved LIDAR system expands Sandia's remote sensing capabilities

For more information:

Technical Contacts:
Shane Sickafoose
505-845-8362
smsicka@sandia.gov

Randy Schmitt
505-844-9519
schmitt@sandia.gov

Science Matters Contact:
Alan Burns
505-844-9642
aburns@sandia.gov

LIDAR (Light Detection and Ranging) systems are now a key component in the Department of Defense (DoD) strategy to protect troops from biological weapons on the battlefield. A LIDAR is a laser optical system capable of detecting aerosol clouds from a remote distance. Analysis of the return signal can determine if the detected aerosol clouds are hazardous biological warfare agents, or simply harmless dust, pollen, or engine exhaust. These "standoff" detection systems can only be tested against aerosol clouds of biological simulants, not against the real threat agents. Thus field test optical backscatter and laser-induced fluorescence data is collected on simulant clouds and the performance is calculated using optical cross section values for the simulants and threat agents.

Recently, Sandia has added optical cross section measurement capability in the long-wave infrared (LWIR) region of 9.3-10.7 μm, a key wavelength region for a biological system now under consideration by the DoD. A tunable, pulsed CO_2 laser, programmed to tune over nineteen discrete wavelengths in the 9.3-10.7 μm region, was added to the Sandia LIDAR facility (a trailer that can be moved to remote locations). One of the major challenges in making the LWIR cross section measurements was that cross sections at visible and near infrared (NIR) laser wavelengths also had to be measured at the same time. The multiple wavelengths required a new beam combiner for the out-going lasers that was able to transmit (coaxially) 355 nm, 1064 nm, and 9.2-10.7 μm laser radiation, and a new receiving wavelength separator to send the returning signals to the wavelength appropriate detectors. An optical-grade Si wafer was used to combine the outgoing laser beams. The LWIR beam from the tunable CO_2 laser was transmitted through the Si wafer at Brewster's angle while the 1064- and 355-nm beams from the Nd:YAG

laser were reflected from it. On the receiver, a custom dielectric coating was used to separate the LWIR return from the other wavelengths. Figure 1 is a schematic of the redesigned optical layout.

To measure agent cross sections, Sandia researchers first collect standoff LIDAR data for aerosol clouds of simulants released in a controlled outdoor facility. After calibration of the LIDAR system, they calculate the optical cross sections of these simulant aerosols. Next, they measure the optical response at all of the wavelengths of the simulant materials and actual threat agents contained in specially-designed stainless steel cuvettes (shown in Figure 2), having a ZnSe window on one side for LWIR optical access and a fused silica window on the other side for UV–NIR optical access. Finally, they compute the agent cross sections by comparing their optical signals relative to that of the simulants using the knowledge gained earlier. It should be noted that the LIDAR trailer is capable of propagating laser radiation for both stand-off field measurements and, after minimal reconfiguration, performing in-trailer measurements on the same materials contained in sample cuvettes with the same laser sources and detectors.

In this way, Sandia will determine the elastic backscatter optical cross sections at twenty-one separate wavelengths, as well as the fluorescence cross sections excited at 355 nm for twenty-four different biological simulants and eight threat agents. These optical cross section values will then be delivered to a DoD customer by early 2010, and will allow the DoD Joint Biological Standoff Detection Systems program to evaluate performance of proposed LIDAR systems to protect troops from biological weapons on the battlefield. This project is a good example of how Sandia laser and optical science expertise and facilities are being used to support a national (engineering) program to develop defenses against biological weapons.

Figure 2: Specially-designed stainless steel cuvette with ZnSe window for LWIR wavelengths and a fused silica window for UV–NIR wavelengths.

Portable Sensor System for the Analysis of Hazardous Chemicals in Water

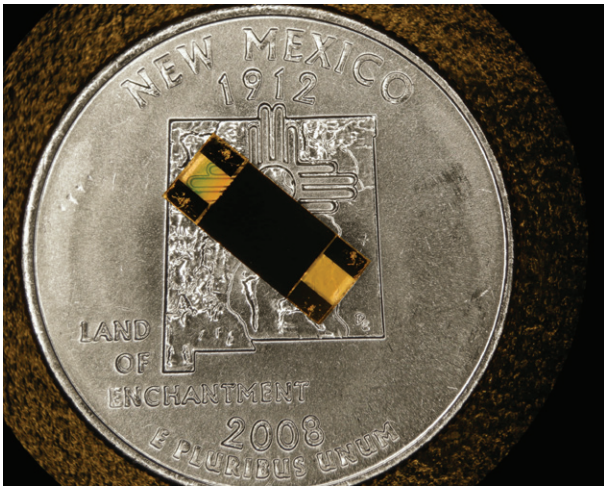

Figure 1: Photo of an NPC-coated 100 MHz SAW device on a quarter. Electrical contacts are made to the four large gold pads. The gold transducer lines between them generate and detect the acoustic wave.

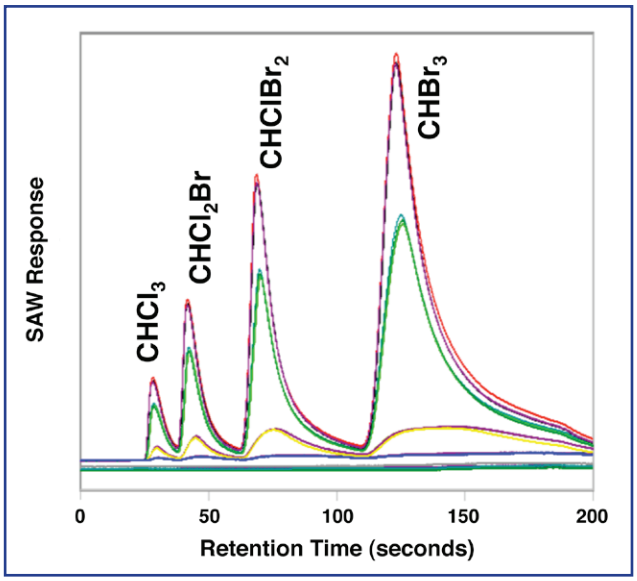

Figure 2: Phase-shift response from an NPC-coated SAW device for controlled exposures to various concentrations of THM mixtures. The retention time is from the gas chromatograph.

Nanoporous-carbon coatings on SAW devices enhance contaminate detection sensitivity by several orders of magnitude

For more information:

Technical Contact:
Michael Siegal
505-845-945
mpsiega@sandia.gov

Science Matters Contact:
Alan Burns
505-844-9642
aburns@sandia.gov

Two hundred million people in the U.S. rely on public utilities for safe, clean water. One hundred years ago, typhoid and cholera epidemics were common throughout our cities; disinfection processes eventually reduced these occurrences. In 1990, the Environmental Protection Agency (EPA) cited drinking water contamination as a major risk and indicated that disease-causing microbes (bacteria, protozoa, and viruses) were the greatest remaining health management challenge for drinking water suppliers. Indeed, over 500,000 cases of waterborne diseases in the U.S. were reported between 1980 and 1994. In 1993, a Milwaukee outbreak of a microbial pathogen, *cryptosporidium*, caused at least 50 deaths.

Ironically, antimicrobial treatment chemicals (*e.g.*, chlorine) react in water with trace natural organic matter to create chemicals, such as trihalomethanes (THMs), which are also hazardous to the public. Epidemiological and toxicological studies of high THM doses demonstrate adverse reproductive and developmental effects, while low dose studies are associated with bladder, rectal and colon cancers. Thus a major challenge for water suppliers is to balance the risks associated with microbial pathogens and the disinfection byproducts. The four THMs (chloroform, dichlorobromomethane, dibromochloromethane, and bromoform) are regulated by the EPA to a total maximum annual average of 80 parts-per-billion (ppb). Due to the difficulty in providing low-cost, simultaneous, individual measurements of each THM, all four THMs are regulated and reported together as a group on either a quarterly or yearly basis, depending on the size of the water utility. Existing THM detection methods for simultaneous,

Sandia National Laboratories

National Nuclear Security Administration

individual measurements use large and expensive equipment, such as mass spectrometry.

To solve this detection problem, Sandia and Parker-Hannifin teamed up to develop a low-cost, portable, highly-sensitive system for simultaneous, individual hazardous chemical detection in water. It uses a purge and trap technique, followed by isothermal gas chromatography that separates the four THMs that are then detected with a nanoporous-carbon (NPC) coated 100 MHz surface acoustic wave (SAW) sensor device fabricated on a quartz crystal (Figure 1). As the separated chemicals sorb into the coated surface and add weight, the SAW sensor measures a reduction in the speed of a sound wave launched from one side of the crystal to the other. The device responds as a function of analyte concentration, measured as a phase shift in the wave over a fixed length. The NPC coatings greatly increase device response by enhancing the available surface area for chemical sorption. NPC coatings are reproducible, sensitive, thermally and chemically stable for long-term use, and appear to outperform all other known coating materials by several orders-of-magnitude (References 1,2).

Figure 2 demonstrates the detection of each THM from fixed mixtures that are separated via gas chromatography and detected by the SAW device. Chloroform elutes first, followed in succession by each chemical in order of molecular weight. The integrated response peaks are plotted versus the known concentration for each THM in Figure 3. A functional power-law behavior demonstrates that NPC-coated SAW devices have limits of detection less than 1 ppb for chloroform, and nearly 1 part-per-trillion for bromoform. Figure 4 illustrates the compact portable prototype system from Parker-Hannifin.

The low-cost, portable system for hazardous chemical detection represents a great advance for the health and safety of the public's clean water supply. It is the only portable sensor system with ppb detection levels and separability of all four THMs, greatly enhancing the information necessary for epidemiological and toxicological studies of these hazardous materials. Furthermore, tests demonstrate the ability to readily detect at least nine different chemicals in a typical water sample. Calibration for these chemicals will enable the device to monitor each contaminant individually.

References

1. M. P. Siegal, W. G. Yelton, D. L. Overmyer, and P. P. Provencio, "Nanoporous carbon films for gas microsensors", *Langmuir*, **20**, 1194 (2004).
2. M. P. Siegal and W. G. Yelton, "Nanoporous-carbon coatings for gas-phase chemical microsensors", *Advances in Science and Technology*, **48**, 161 (2006).

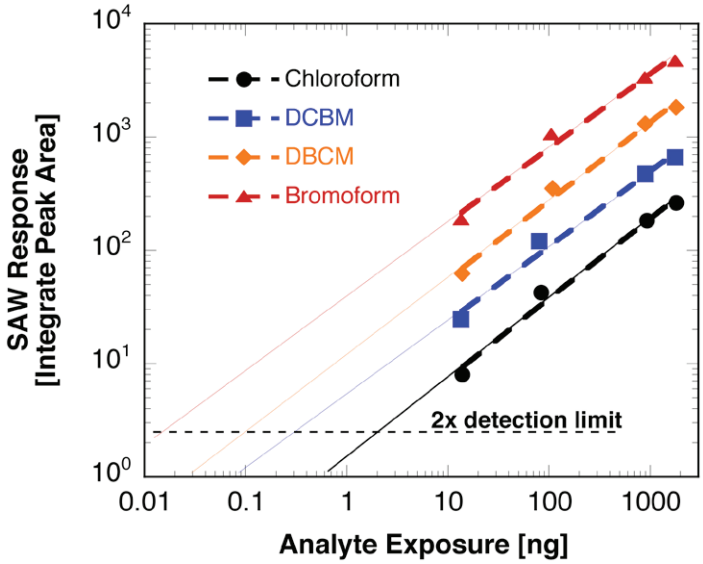

Figure 3: SAW response vs. analyte exposure. (Note: 12 ng ~ 1 ppb.) The dashed line represents the SAW device detection limit, due to signal-to-noise. The detection limits for $CHCl_3$, $CHCl_2Br$, $CHClBr_2$ and $CHBr_3$ are 0.16, 0.026, 0.009, and 0.001 ppb, respectively.

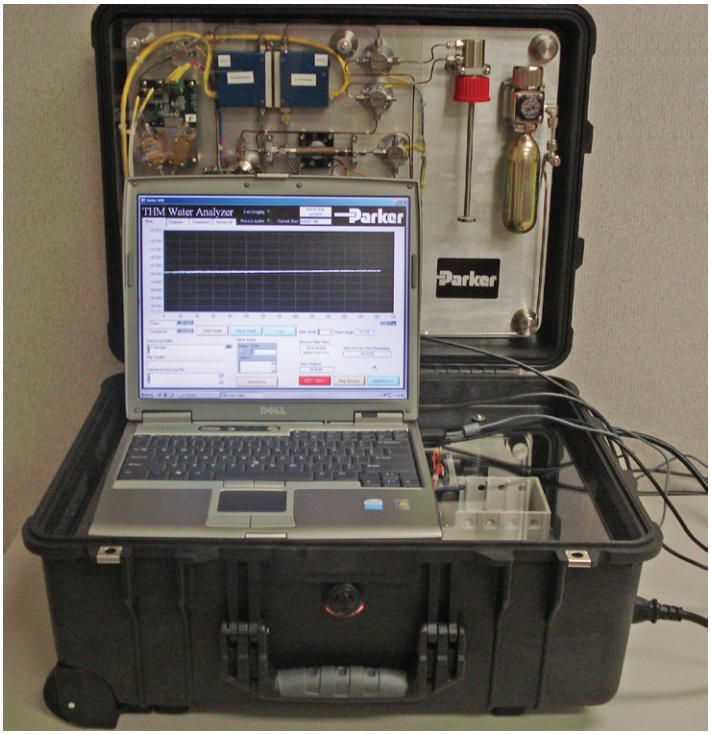

Figure 4: Briefcase version of portable detection system built by Parker-Hannifin that includes power supply, laptop computer, water sampling, purge and trap, isothermal chromatography, and SAW sensors for detection.

Microelectronics and Microsystems
Microelectromechanical Devices

Zero Power Acoustic Signal Processing

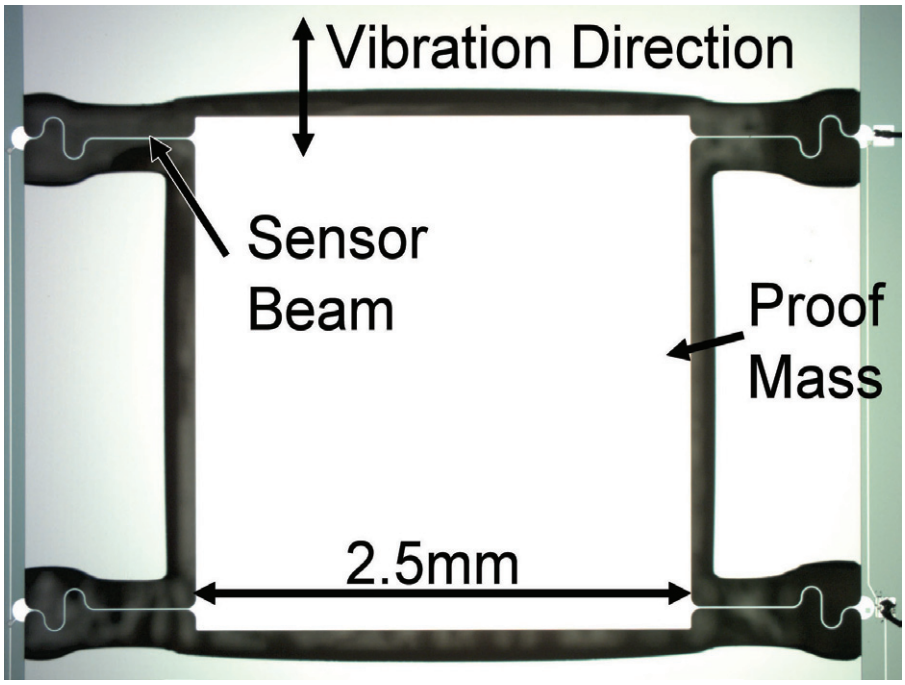

Figure 1: Photograph of zero power, 500 Hz vibration sensor. The 2.5 X 2.5 mm proof mass (coated with reflective metal) is supported at each corner by a sensor beam.

Pre-processing signals in the acoustic domain can eliminate stand-by power in certain classes of autonomous sensors

For more information:

Technical Contact:
Roy Olsson
505-284-6375
rholsso@sandia.gov

Science Matters Contact:
Alan Burns
505-844-9642
aburns@sandia.gov

Eliminating standby power is critical to extending the lifetime and to reducing the size of unattended sensors. Ideally, an autonomous sensor system would remain in standby consuming zero power until an event triggers power-up of the entire device for data logging, processing or transmission. In reality, however, processing the wake-up event often requires significant power consumption, particularly for complex event signatures, which limits device lifetime and size. Sandia is developing a microelectromechanical (MEMS) circuit capable of processing complex vibration signatures while consuming near zero power.

The wake-up circuit operates via piezoelectric transduction of mechanical vibration that produces an output current proportional to the mechanical displacement. When no vibration is present, there is zero displacement, zero output current and zero power consumption. Under vibration, a strain induced in a thin-film piezoelectric layer produces a current that is passed through a circuit to create a voltage that must be large enough to turn on a transistor. Since the displacement and piezoelectric output current can be engineered to respond only to certain vibration frequencies, complex vibration profiles can be programmed into the wake-up circuit and processed in the mechanical domain without consuming power. This technology is readily extendable to zero power processing of radio frequency signals as well. The major challenges being addressed are: (1) covering the frequency range of interest in a single microfabrication process, and (2) realizing a large enough voltage signal swing to trigger microsystem wake-up in an event while consuming zero power in standby.

A micromachined 500 Hz vibration sensor is shown in Figure 1. It is fabricated in a 5-mask process in Sandia's MESA (Microsystems and Engineering Sciences Applications) facility capable of producing sensors and sensor arrays operating from 100 Hz to 10 kHz. The sensor consists of a tiny 0.3 mm^3 proof mass suspended from the silicon wafer by four 1-mm-long serpentine sensor beams. The resonant vibration frequency and amplitude response of the sensor are engineered by setting the proof mass size, sensor beam length, and the size of the serpentine. In the presence of a vibration, the sensor will vibrate back and forth in the direction shown in Figure 1. If the frequency of vibration is resonant with the sensor, the magnitude of the sensor displacement will be amplified by approximately 500 times.

A cross-section of a sensor beam and zero power circuit schematic are shown

Sandia National Laboratories

LDRD LABORATORY DIRECTED RESEARCH & DEVELOPMENT

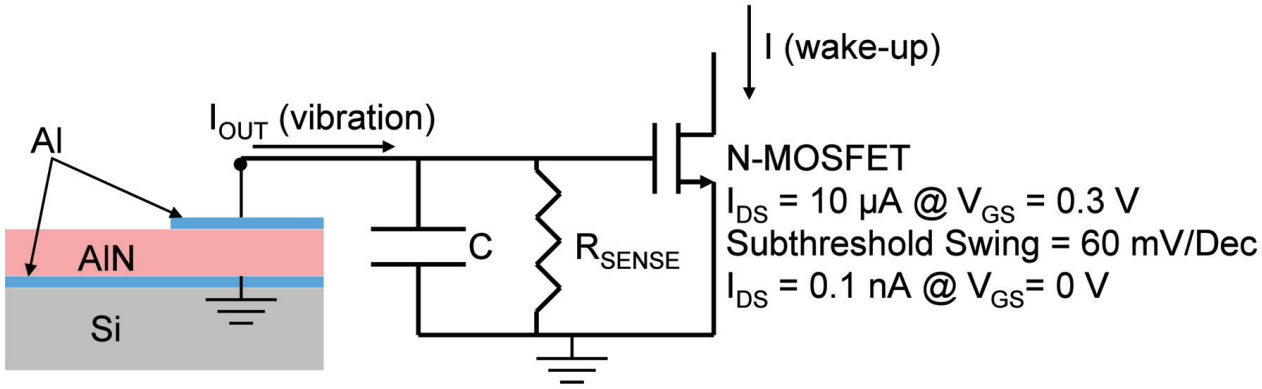

Figure 2: Sensor beam cross-section and zero power circuit schematic.

in Figure 2. Under vibration, the displaced sensor beams create strain in the thin film piezoelectric aluminum nitride (AlN) layer. The piezoelectric effect converts the strain into an output current that is proportional to both sensor displacement and vibration frequency and is subsequently converted into a voltage. The maximum voltage for a given displacement amplitude is limited by the piezoelectric constant of AlN and the parasitic capacitance of the sensor; thus high quality piezoelectric thin films are vital for achieving high output voltages.

Figure 3 shows the modeled response of the 500 Hz sensor in Figure 1 *vs*. frequency for an input vibration of 0.1 G, where 1 G is the acceleration due to gravity at sea level. The resonance of the sensor at 500 Hz is clearly seen as the output sensor voltage reaches 0.7 V for a maximum sensor displacement of only 50 µm. A typical MOSFET (metal-oxide field effect) transistor shown in Figure 2 will turn on when the input voltage exceeds the threshold (in this case 0.3 V), but will consume as little as 0.1 nA when no vibration-induced voltage is present. Based on finite element modeling, the zero power sensor system currently in development will be capable of processing vibration signals as low as 10 milliG. To date, Sandia has produced an array of four sensors operating at 500, 667, 834 and 1000 Hz that occupies a total volume of 0.5 mm^3.

Potential applications of unattended, zero power vibration sensors include the monitoring of machinery such as industrial equipment, airplanes and automobiles, where abnormal vibration profiles measured in key locations can be an early sign of failure. Other applications include circumstances where sensors must be automonously deployed for long periods without the need for maintenance such as changing batteries.

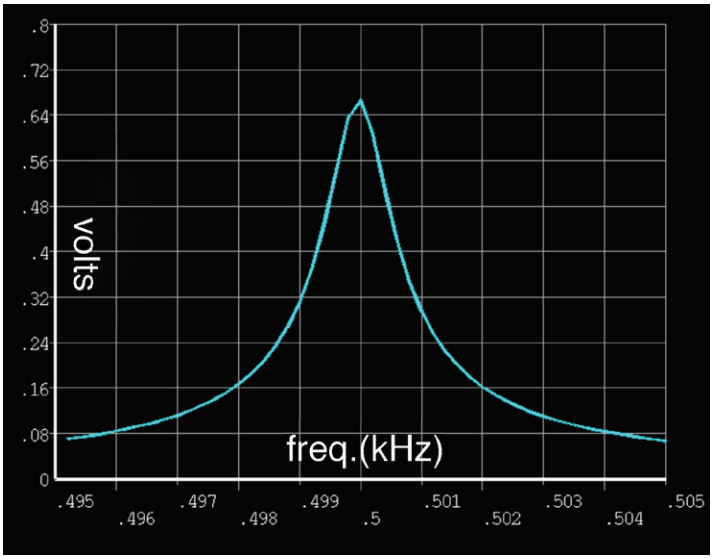

Figure 3: Finite element model predicted response of the sensor in Figure 1 under a 100 milli-G vibration *vs*. vibration frequency.

$H_2S + 2Cu \rightarrow$

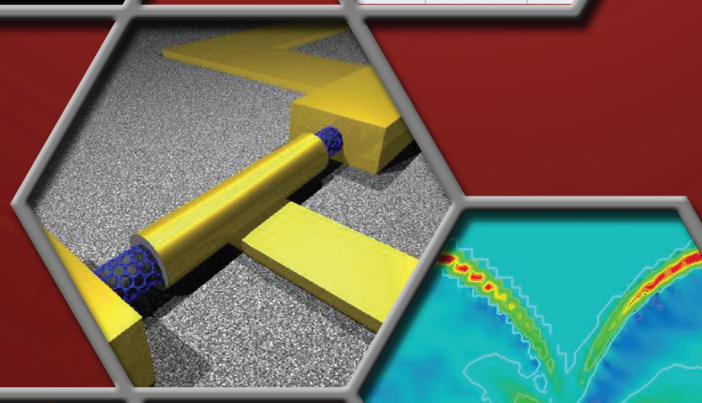

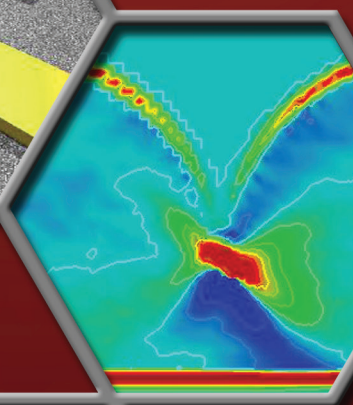

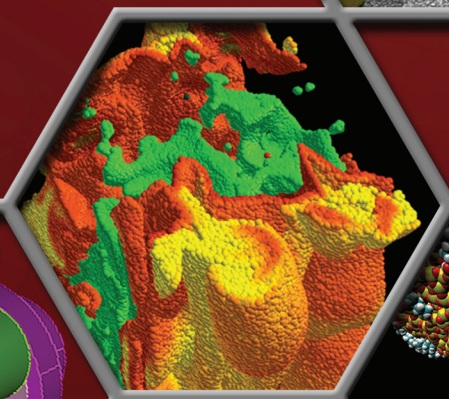

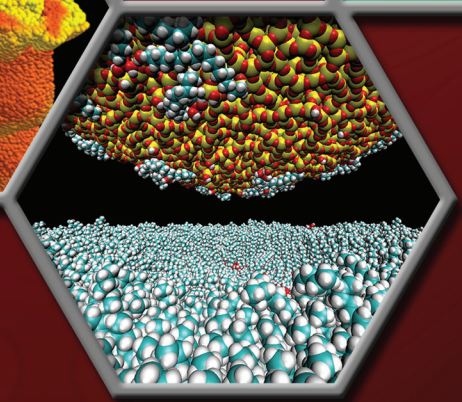

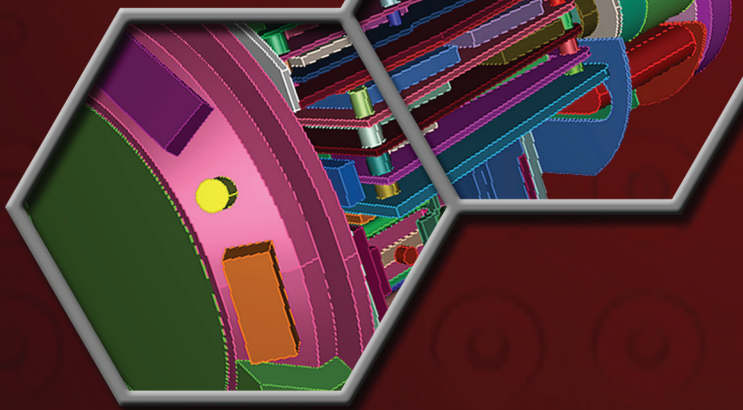

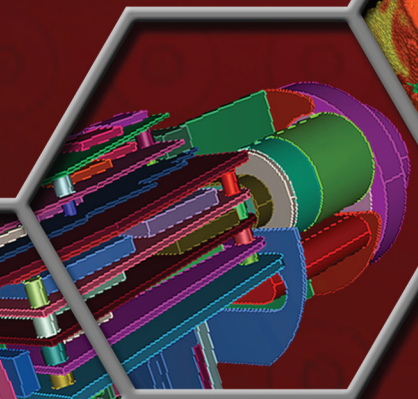

National Nuclear Security Administration

LDRD